Review

Antimonide-based compound semiconductors for electronic devices: A review

Brian R. Bennett *, Richard Magno, J. Brad Boos, Walter Kruppa, Mario G. Ancona

Electronics Science and Technology Division, Naval Research Laboratory, Washington, DC 20375-5347, USA

Abstract

Several research groups have been actively pursuing antimonide-based electronic devices in recent years. The advantage of narrow-bandgap Sb-based devices over conventional GaAs- or InP-based devices is the attainment of high-frequency operation with much lower power consumption. This paper will review the progress on three antimonide-based electronic devices: high electron mobility transistors (HEMTs), resonant tunneling diodes (RTDs), and heterojunction bipolar transistors (HBTs). Progress on the HEMT includes the demonstration of Ka- and W-band low-noise amplifier circuits that operate at less than one-third the power of similar InP-based circuits. The RTDs exhibit excellent figures of merit but, like their InP- and GaAs-based counterparts, are waiting for a viable commercial application. Several approaches are being investigated for HBTs, with circuits reported using InAs and InGaAs bases.
Published by Elsevier Ltd.

Contents

---

* Corresponding author. Tel.: +1 202 767 3665; fax: +1 202 767 1165.
  E-mail address: brian.bennett@nrl.navy.mil (B.R. Bennett).

Report Documentation Page		*Form Approved* *OMB No. 0704-0188*

Public reporting burden for the collection of information is estimated to average 1 hour per response, including the time for reviewing instructions, searching existing data sources, gathering and maintaining the data needed, and completing and reviewing the collection of information. Send comments regarding this burden estimate or any other aspect of this collection of information, including suggestions for reducing this burden, to Washington Headquarters Services, Directorate for Information Operations and Reports, 1215 Jefferson Davis Highway, Suite 1204, Arlington VA 22202-4302. Respondents should be aware that notwithstanding any other provision of law, no person shall be subject to a penalty for failing to comply with a collection of information if it does not display a currently valid OMB control number.

1. REPORT DATE **APR 2005**	2. REPORT TYPE	3. DATES COVERED **00-00-2005 to 00-00-2005**
4. TITLE AND SUBTITLE **Antimonide-based compound semiconductors for electronic devices: A review**		5a. CONTRACT NUMBER
		5b. GRANT NUMBER
		5c. PROGRAM ELEMENT NUMBER
6. AUTHOR(S)		5d. PROJECT NUMBER
		5e. TASK NUMBER
		5f. WORK UNIT NUMBER
7. PERFORMING ORGANIZATION NAME(S) AND ADDRESS(ES) **Naval Research Laboratory,Electronics Science and Technology Division,4555 Overlook Avenue SW,Washington,DC,20375**		8. PERFORMING ORGANIZATION REPORT NUMBER
9. SPONSORING/MONITORING AGENCY NAME(S) AND ADDRESS(ES)		10. SPONSOR/MONITOR'S ACRONYM(S)
		11. SPONSOR/MONITOR'S REPORT NUMBER(S)
12. DISTRIBUTION/AVAILABILITY STATEMENT **Approved for public release; distribution unlimited**		
13. SUPPLEMENTARY NOTES		

14. ABSTRACT

Several research groups have been actively pursuing antimonide-based electronic devices in recent years. The advantage of narrowbandgap Sb-based devices over conventional GaAs- or InP-based devices is the attainment of high-frequency operation with much lower power consumption. This paper will review the progress on three antimonide-based electronic devices: high electron mobility transistors (HEMTs), resonant tunneling diodes (RTDs), and heterojunction bipolar transistors (HBTs). Progress on the HEMT includes the demonstration of Ka- and W-band low-noise amplifier circuits that operate at less than one-third the power of similar InP-based circuits. The RTDs exhibit excellent figures of merit but, like their InP- and GaAs-based counterparts, are waiting for a viable commercial application. Several approaches are being investigated for HBTs, with circuits reported using InAs and InGaAs bases.

15. SUBJECT TERMS					
16. SECURITY CLASSIFICATION OF:			17. LIMITATION OF ABSTRACT	18. NUMBER OF PAGES	19a. NAME OF RESPONSIBLE PERSON
a. REPORT **unclassified**	b. ABSTRACT **unclassified**	c. THIS PAGE **unclassified**	**Same as Report (SAR)**	**21**	

Standard Form 298 (Rev. 8-98)
Prescribed by ANSI Std Z39-18

1. Introduction

The binary compound semiconductors AlSb, GaSb, InSb, and InAs along with their related alloys are candidates for high-speed, low-power electronic devices. Applications could include high-speed analog and digital systems used for data processing, communications, imaging, and sensing, particularly in portable equipment such as hand-held devices and satellites. The development of Sb-based transistors for use in low-noise high-frequency amplifiers, digital circuits, and mixed-signal circuits could provide the enabling technology needed to address these rapidly expanding needs. In Fig. 1, we show the trend toward higher frequencies and lower power consumption with increasing lattice constant. In recent years, considerable progress has been made in HEMTs, RTDs, and HBTs in the antimonide–arsenide materials system (lattice constants greater than 6.0 Å). In this paper, we will review the progress in the design, growth, fabrication, and performance of these electronic devices. We will discuss our work at NRL as well as major results from other groups.

2. InAs quantum wells and high-electron-mobility transistors

2.1. Background

The first high electron mobility transistors (HEMTs) were fabricated with GaAs channels and AlGaAs barriers [1]. These devices are also known as modulation-doped field effect transistors (MODFETs). In order to achieve higher electron mobility and velocity (translating to higher frequency operation), In was added to the channel. Typical structures have $In_{0.2}Ga_{0.8}As$ channels that are *pseudomorphically* strained to the GaAs lattice constant (PHEMTs). In order to improve performance further, additional In was added to the channel and the barrier material was changed to InAlAs; the larger lattice constants were accommodated by using InP substrates. The logical progression of this trend is to use pure InAs as the channel along with nearly lattice-matched AlSb, AlGaSb, or InAlSb for the confining layer as the arsenides are not suitable barriers. Advantages of this material system include the high electron mobility (30,000 cm^2/V s at 300 K) and
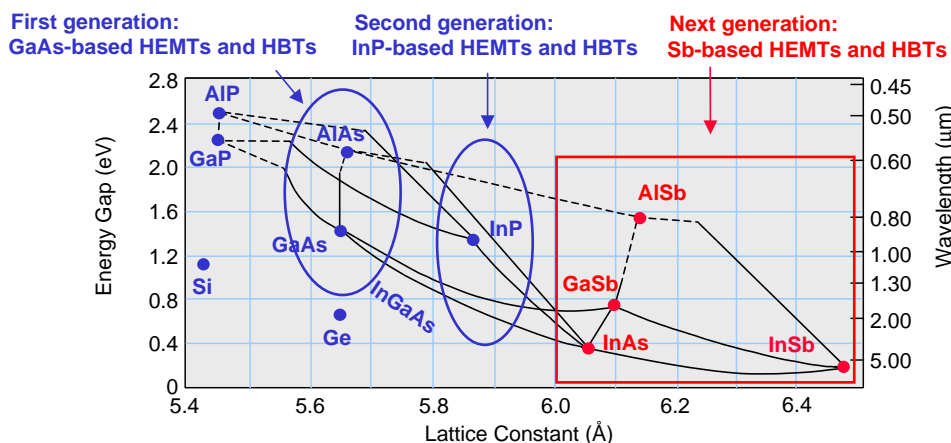

Fig. 1. Energy gap versus lattice constant, showing the evolution of transistors to larger lattice constants and smaller bandgaps for high-frequency and low-power operation.
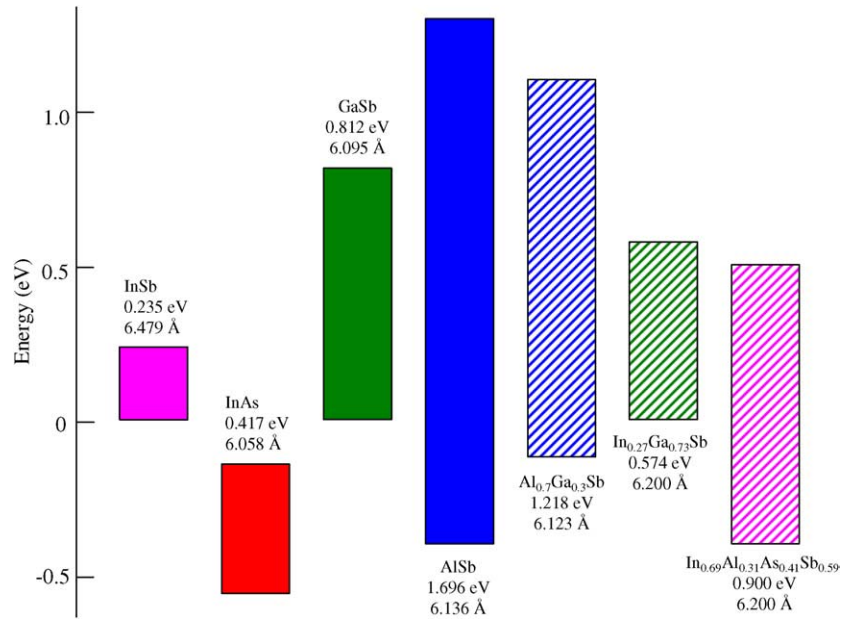
Fig. 2. Band alignments for selected binary and alloy semiconductors at 0 K.

velocity (4×10^7 cm/s) of InAs [2], and a large conduction band offset between InAs and AlSb (1.35 eV), as shown in Fig. 2 [3–6].

2.2. InAs/AlSb single quantum wells

Most of the recent advances in antimonide-based HEMTs have involved heterostructures grown by molecular beam epitaxy (MBE). Antimonide growth by MBE was first reported in the late 1970s [7–9]. The growth of antimonide and mixed antimonide/arsenide structures by MBE has presented some challenges compared to growth of arsenides [10]. For the most part, solutions have been found. Overall, growth of antimonides is simpler than nitrides and does not present the safety issues associated with phosphides. Scale-up to production MBE systems should be feasible.

Crucial advances for transistor applications were reported by Prof. Kroemer's group at the University of California at Santa Barbara (UCSB), beginning in the late 1980s. They grew InAs/AlSb single quantum wells and showed that high mobilities could be achieved by controlling the interfaces [11,12]. The interface bonds can be either InSb-like or AlAs-like as there is no common cation or anion for a heterojunction between InAs and AlSb. Work by Tuttle et al. showed that the bottom interface must be InSb-like to achieve high mobilities. Bolognesi et al. varied the thickness of the InAs quantum well and achieved high mobilities for 125–200 Å [13]. The mobility of thinner wells was suppressed by interface scattering. The decrease in mobility for wells thicker than 200 Å presumably resulted from the formation of misfit dislocations due to the 1.3% lattice mismatch between the InAs and AlSb.

Although it is not the focus of this review, we note that the growth of InAs quantum wells with very high mobilities

has lead to many interesting physics studies. For example, see work on ballistic transport phenomena [14,15]. In addition, the Hall effect in these structures is of interest for magnetic sensing [16–18] and magnetoelectronic logic applications [19].

2.3. Doping of HEMTs

Key parameters for HEMT quantum wells are electron mobility and sheet carrier density. Sheet carrier concentrations for unintentionally doped InAs/AlSb single quantum wells are known to be a function of the thickness of the upper barrier, the cap material (usually InAs or GaSb), the interface bond type, and the purity of the AlSb. In most cases, the undoped heterostructures are n-type with densities less than or approximately equal to 1×10^{12}/cm^2 [20]. Higher sheet charge densities are typically desirable for HEMT applications. The arsenic-soak technique, first reported by Tuttle et al., is one way to enhance the sheet carrier concentration. After growing an InAs quantum well and an AlSb spacer layer, the AlSb is subjected to an As beam [12]. Apparently, As atoms replace Al atoms, providing extra electrons to the conduction band. Densities of $1–2 \times 10^{12}$/cm^2 are typically achieved. High-speed HEMTs have been fabricated using this technique [21].

Silicon is the most common n-type dopant in III–V MBE systems. However, it is amphoteric in the III–V's, producing n-type GaAs, InAs, AlAs, and InSb, but p-type GaSb and AlSb on (100) surfaces [22]. Sasa et al. achieved sheet carrier concentrations in the $2–4 \times 10^{12}$/cm^2 range by Si planar doping in an 18 Å InAs quantum well located 80 Å below a 150 Å InAs quantum well clad by AlGaSb [23]. The energy levels in the very thin doped well are higher than in the channel due to quantum confinement.

Hence, electrons will transfer into the channel. This technique has been successfully applied to InAs HEMTs by at least three groups [24–27].

Chalcogens such as S, Se, and Te are in column VI of the periodic table and hence logical candidates for n-type dopants in III–V semiconductors. As discussed by Furukawa and Mizuta [28], elemental sources such as Te have a very high vapor pressure and hence are not suitable for III–V MBE. An alternative is to use chalcogenides such as PbSe and GaTe. Wood demonstrated n-type doping of GaAs using PbSe and PbS [29]. Furukawa and Mizuta successfully used GaTe to make n-type AlGaSb layers in a transistor [28]. Subbanna et al. used PbTe to achieve controllable carrier concentrations from 10^{16} to $10^{18}/cm^3$ in a detailed doping study of AlSb and GaSb [30]. Several groups have successfully used GaTe as a dopant source for Sb-based transistors and other structures [31–33].

The relationship between mobility and carrier density is plotted in Fig. 3 for several undoped, Si-doped, and Te-doped HEMT structures grown at NRL. High mobility and low sheet resistance are desired for HEMT applications. Unfortunately, the highest mobilities are achieved for undoped structures with carrier densities that are too low to achieve sheet resistances less than 200 $\Omega/\square$. Fig. 3 demonstrates that sheet resistances near 100 $\Omega/\square$ have been reached for both Si- and Te-doping. We find that densities near $3.0 \times 10^{12}/cm^2$ are optimal for achieving both high mobility and low sheet resistance. Note that these high mobilities and low sheet resistances cannot be achieved by GaAs- or InP-based HEMTs. Other groups have achieved results similar to those shown in Fig. 3. To our knowledge, no one has achieved the highest mobilities and high densities simultaneously (e.g. 25,000–30,000 cm^2/V s and $\sim3 \times 10^{12}/cm^2$). Based upon Shubnikov-de Haas measurements, electrons begin to populate a second sub-band in InAs quantum wells at densities of $1.4–2.4 \times 10^{12}/cm^2$ [23,26,34]. Hence, for higher densities we expect intersubband scattering and a reduction in mobility, as shown in Fig. 3.

Both Si and Te doping appear to be viable for InAs HEMTs. Advantages of Si include the fact that it is more often available in MBE systems and has a much lower vapor pressure, meaning that source depletion is generally not a problem. A disadvantage of Si is that a decrease in growth temperature may be required between the InAs channel and the doped layer [26]. For Te doping, a constant growth temperature can be used. In addition, Te should act as a donor in any AsSb alloy.

2.4. HEMT design and performance

The layer structure and calculated band structure for a HEMT with Te delta-doping are illustrated in Fig. 4. Semi-insulating GaAs substrates are typically used for InAs HEMTs as there are no suitable zincblende insulating substrates with lattice constants near 6.1 Å. The 1.7 μm
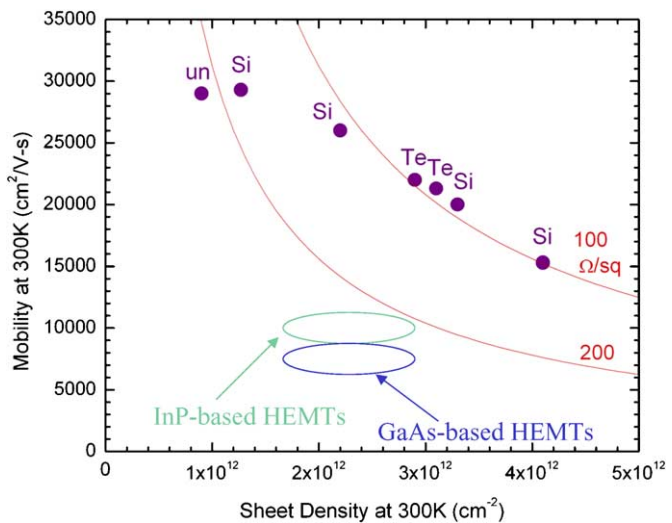

Fig. 3. Electron mobility versus sheet density for InAs single quantum wells. The doping technique is indicated next to each point. Ranges for typical GaAs- and InP-based HEMTs are also indicated.
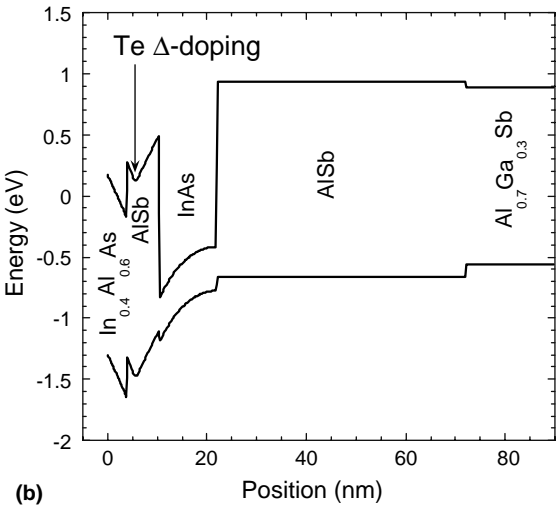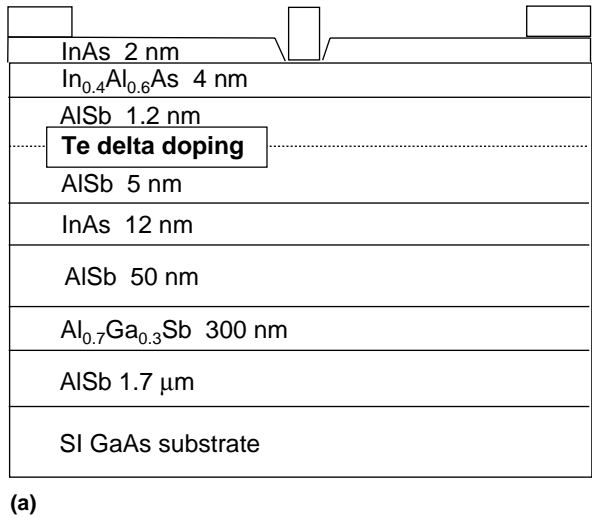

Fig. 4. Heterostructure cross-section (a) and calculated band structure (b) for InAs HEMT with Te delta-doping.

buffer layer of AlSb is almost fully relaxed and accommodates the 8% lattice mismatch [35]. The 0.3 μm layer of $Al_{0.70}Ga_{0.30}Sb$ allows for a mesa isolation etch that stops in the AlGaSb and hence does not expose AlSb outside the active region to air or moisture that will cause it to deteriorate [36–38]. The InAlAs layer enhances the insulating properties of the barrier by providing a barrier to holes. In addition, it serves as an etch-stop, enabling a gate recess etch to be employed [21]. Despite the large lattice mismatch and three-dimensional growth, the InAlAs layer does not degrade the electron mobility, presumably because it is at least 50 Å above the channel. The AlGaSb and InAlAs layers are now used by at least three groups investigating InAs HEMTs [33,37,39].

The uniformity of transistors across a wafer will be important for circuit applications. Non-uniformities can be introduced in the growth or subsequent processing. Contactless resistivity mapping of an as-grown wafer can easily be done with a Lehighton system as a test of uniformity. We have measured non-uniformities as low as 0.7% across a 3-in. wafer (typical values were 1–3%) for Te-delta-doped structures similar to the one in Fig. 4, grown on a 3-in. Riber Compact 21T MBE system [35].

The low-power potential of these materials was demonstrated by the fabrication of InAs HEMTs with a 60 nm gate length [40]. The as-grown heterostructure had a sheet density of $1.6 \times 10^{12}/cm^2$ and a mobility of 21,300 cm^2/V s. The I–V characteristics shown in Fig. 5 indicate that the depletion-mode device has a transconductance of 1.1 S/mm at $V_{DS} = 0.35$ V and $V_{GS} = -0.50$ V. The increase in output conductance at a drain voltage above 0.3 V is due to the effects of impact ionization in the channel. At this bias condition, the device exhibits an extrinsic f_T of 160 GHz. The potential for low-voltage operation is demonstrated by the plot of measured f_T as a function of drain voltage in Fig. 6. An f_T of 90 GHz is obtained at a drain voltage of only 0.10 V. InP- and GaAs-based HEMTs cannot reach these high frequencies at such low voltages.

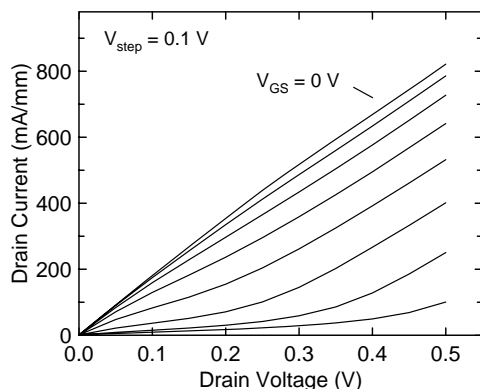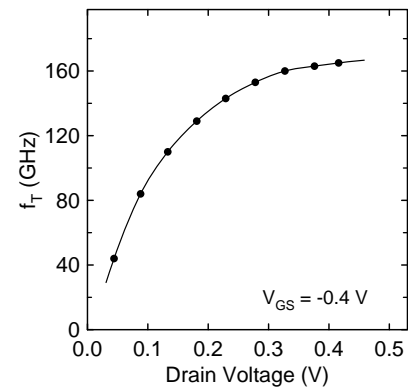In the last three years, funding from the DARPA antimonide-based compound semiconductor (ABCS) program

Fig. 6. Extrinsic cut-off frequency, f_T, versus drain voltage for a 60 nm InAs-channel HEMT. Note that an f_T of 90 GHz is achieved at a bias of only 0.10 V [40]. © 1999, AVS The Science and Technology Society.

has resulted in substantial advances in InAs HEMT technology. A collaboration between the Naval Research Laboratory and Northrop Grumman Space Technology (NGST) focused on making the devices manufacturable. Significant steps in this direction were the elimination of an air bridge used for the device discussed above and the successful fabrication of T-gates. Results from 0.1 μm HEMTs fabricated from a heterostructure with $n_s = 1.3 \times 10^{12}/cm^2$ and $\mu = 29,000$ cm^2/V s are shown in Figs. 7 and 8 [37,41,42]. The devices displayed high transconductance (G_m) at low drain–source voltage (V_{DS}), and low on-state resistance (R_{ON}). The average G_m peak was 1.05 S/mm and 1.6 S/mm measured at a V_{DS} of 0.2 V and 0.3 V, respectively. The average off-state reverse gate-drain breakdown voltage (BV_{GD}) was -1.42 V (measured at a gate current of -1 mA/mm). DC characteristics in Fig. 7 were measured from an 80-μm-gate-width device with typical extrinsic R_{ON} of 0.67 Ω mm. (The high peak for DC $G_m @ V_{DS} = 0.4$ V is anomalous and related, in part, to impact ionization effects.) These characteristics illustrate the combination of low-drain-voltage operation, low knee voltage, and high transconductance, which are critical parameters for low-power, high-frequency operation.

Fig. 5. HEMT drain characteristics for an InAs HEMT with a 60 nm gate length, $L_{DS} = 1.0$ μm, and $W_G = 50$ μm [40]. © 1999, AVS The Science and Technology Society.
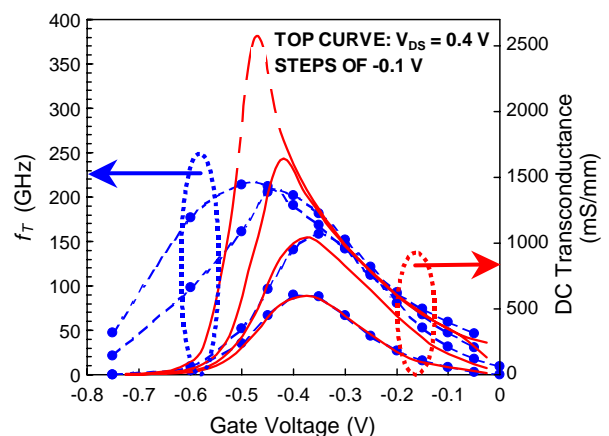
Fig. 7. Extrinsic cut-off frequency, f_T, and DC transconductance versus gate voltage for 0.1 μm T-gate InAs-channel HEMT [37]. © IEEE.
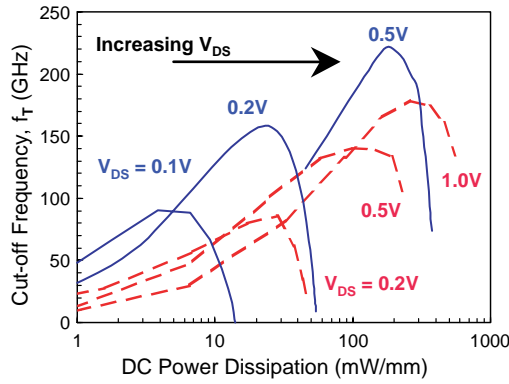
Fig. 8. Extrinsic cut-off frequency, f_T, versus power dissipation for InAs/AlSb HEMT (solid lines) at V_{DS} = 0.1, 0.2, and 0.5 V and InAlAs/InGaAs HEMT (dashed lines) at V_{DS} = 0.2, 0.5, and 1.0 V [37]. © IEEE.

Small signal RF tests were also performed on-wafer, and the maximum available gain was 10 dB at 100 GHz. The normal slope (6 dB/octave) was used to extrapolate beyond 100 GHz and gave an average peak f_T of 153 GHz and 212 GHz at V_{DS} of 0.2 and 0.4 V, and drain current densities of 115 and 340 mA/mm, respectively. These correspond to DC power dissipations of 22 and 180 mW/mm. Compared to f_T-DC power performance of state-of-the-art 0.1-μm gate length InAlAs/InGaAs/InP HEMTs, our AlSb/InAs HEMTs provide equivalent f_T at 5–10 times lower power dissipation, as shown in Fig. 8. The use of a T-gate resulted in values of f_{max} greater than f_T, with f_{max} = 270 GHz at V_{DS} = 0.4 V.

HRL Laboratories recently reported InAs-channel HEMTs with InAlAs barrier layers. The composition and thickness of the $In_xAl_{1-x}As$ is not given, but presumably the layers are In-rich and pseudomorphic. For a 70 nm gate length, an intrinsic f_T of 308 GHz was achieved at V_{DS} = 0.70 V. The peak intrinsic f_{max} was 110 GHz. The device did not have a T-gate [39].

A Rockwell-UCSB team also achieved excellent low-power performance. They report 0.25-μm T-gate HEMTs fabricated from a heterostructure with n_s = 3.7×10^{12}/cm^2 and μ = 19,000 cm^2/V s [33]. The extrinsic values of both f_T and f_{max} are 162 GHz at V_{DS} = 0.35 V, V_{GS} = −1.1 V, I_d = 6.1 mA, and I_g = −20.9 μA. In a subsequent report, 0.1-μm T-gates were written on a heterostructure with n_s = 2.1×10^{12}/cm^2 and μ = 18,000 cm^2/V s. These devices reached an f_T of 235 GHz at V_{DS} = 0.45 V, and an f_{max} of 235 GHz at V_{DS} = 0.30 V, as shown in the contour plots of Fig. 9 [43]. Note that both f_T and f_{max} exceed 100 GHz at a drain bias of only 0.10 V, again highlighting the low-power potential of these transistors.

The threshold voltage of the n_s = 3.7×10^{12}/cm^2 Rockwell device discussed above was −1.2 V. We have also observed large negative threshold voltages (V_{th} < −1.0 V) for some devices with high sheet charge (~3×10^{12}/cm^2). These high threshold voltages are generally not desirable for low-power circuits. One way to make V_{th} less negative is to decrease the sheet density. The disadvantage to this
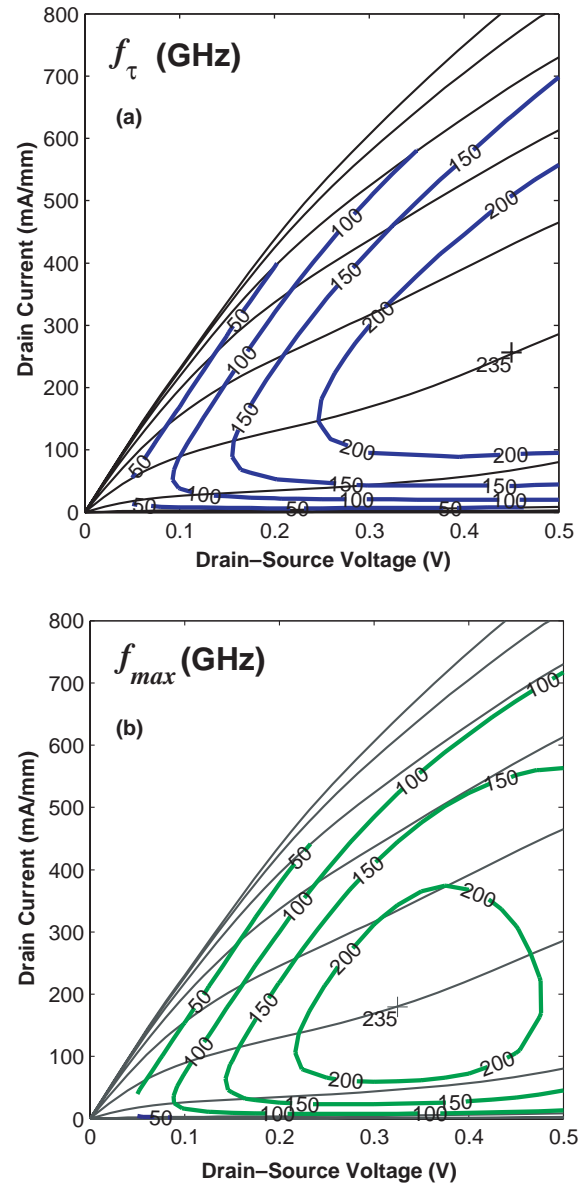
Fig. 9. Drain current versus drain–source voltage for Rockwell 0.1-μm-gate-length, InAs/AlSb HEMT with contours of f_T and f_{max} illustrating high-frequency performance at low power [43]. © IEEE.

approach is evident in Fig. 3. At 3×10^{12}/cm^2, mobilities near 20,000 cm^2/V s are possible, yielding sheet resistances near 100 Ω/□. If the density is reduced to 1×10^{12}/cm^2, the mobility may increase to ~30,000 cm^2/V s, but the sheet resistances will increase to ~200 Ω/□. This will mean higher access resistance for the HEMTs. An alternative is to reduce the gate-to-channel spacing. To quantify this approach, we performed Silvaco modeling of V_{th} as a function of sheet density and vertical spacing. We use the distance between the gate (which rests on the InAlAs) and the center of the channel as a parameter. Surface state and quantum effects are not included. The results are shown in Fig. 10. For low densities, the threshold voltage is small (approximately −0.5 V) regardless of the gate–channel separation. For higher densities, there is only a

Fig. 10. Calculated threshold voltage as a function of sheet charge at three different values of gate-to-center-of-channel separation. Experimental data points are also shown.

small difference between the 162 and 214 Å lines, but a substantial increase in V_{th} for 300 Å. We also include experimental points on the plot which generally confirm the predictions. (We have several measured values of $-0.4 < V_{th} < -0.7$ for 1–2×10^{12}/cm^2 but do not include all of them on the plot for clarity.) It was these results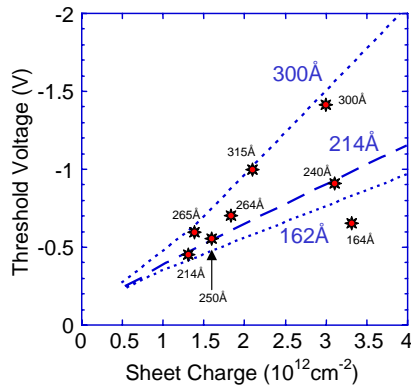, in part, that led us to select the Te-delta-doped structure shown in Fig. 4. Using structures similar to Fig. 4, we have achieved densities of 1–3×10^{12}/cm^2 with gate–channel separations of 130–214 Å. The reduced spacing is also advantageous because it allows good aspect ratios as gate lengths are reduced.

2.5. Variations to standard HEMT design

A number of variations to the InAs HEMTs described above have been investigated over the last decade. Several involve changes to the channel. Yang et al. fabricated FETs from a heterostructure with an 80 Å InAs/50 Å GaSb composite channel [44]. By varying the gate voltage, the carriers in the channel can be changed from electrons to holes, resulting in a novel V-shaped transfer characteristic. Boos et al. modified the conventional InAs HEMTs by adding a 42 Å InAs subchannel, separated from the 100 Å InAs channel by 30 Å AlSb [45]. The subchannel has a larger bandgap than the channel due to quantization. Hot electrons can tunnel from the channel into the subchannel before gaining enough kinetic energy for impact ionization. HEMTs using this design exhibited an intrinsic f_T of 250 GHz for a 0.1 µm gate length. A similar approach was taken by Lin et al. who used a composite channel of InAs and InAsP (InAlAs) with the InAsP (InAlAs) having a larger bandgap [46,47]. The resulting HEMTs exhibited increased breakdown voltage compared to InAs-channel devices. A final variation to the channel is to incorporate alloys of InAsSb. Using digital alloys of InAsSb, we showed that the band alignment between the InAs$_{1-x}$Sb$_x$ and AlSb changes to type-I for $x > 0.15$ [48]. The type-I alignment should enable better confinement of holes generated thermally or as a result of impact ionization in the

channel. We fabricated 0.1 µm HEMTs with InAs$_{0.8}$Sb$_{0.2}$ channels and achieved intrinsic values of $f_T = 180$ GHz and $f_{max} = 120$ GHz, and a voltage gain of 9, despite the fact that the mobility was only 13,400 cm^2/V s [49]. More recently, we have improved the mobility to 22,000 cm^2/V s using random alloys of InAs$_{0.7}$Sb$_{0.3}$ and barriers of In$_{0.2}$Al$_{0.8}$Sb. Transconductances of 1.35 S/mm were measured at $V_{DS} = 0.3$ V for a 0.2 µm gate length [50,51].

Another variation we investigated included a 100–200 Å layer of p-type GaSb (doped in the mid 10^{17}/cm^3 by Si or Be) 500 Å below the InAs channel [21]. The intention of this layer is to drain a portion of the impact-ionization-generated holes back to the source contact rather than having them remain in the AlSb buffer layer where they are likely to cause deleterious trapping effects or be collected at the gate contact and thereby increase the gate leakage current. A related technique is to use an epitaxial back-gate placed below the quantum well to remove holes [52].

Another method to minimize impact ionization effects is the use of dual gates. The use of a dual gate for InAs HEMTs was proposed in 1990 [53] and demonstrated by two groups in 1996 [54,55]. This design enables the reduction of leakage current by using a second gate to modify the E-field under the first gate. A disadvantage is the increased process complexity required to achieve low access resistance with the dual-gate design.

As mentioned earlier, even undoped InAs quantum wells usually have $\sim 10^{12}$/cm^2 electrons in the channel. Hence, InAs HEMTs normally operate as depletion-mode devices. Zhao et al. incorporated Be delta-doping in the upper barrier to achieve n-channel enhancement-mode transistors [56]. Recently, other groups have also been working toward this goal [39,57,58].

The typical InAs HEMT structures include a thin (~ 2 nm) fully-depleted InAs cap which is removed to allow a recessed gate on the InAlAs barrier. An alternative, commonly used in InP-based HEMTs, is to grow a thicker n$^+$ cap layer. This can result in low access resistance and low threshold voltage. In a recent report, HEMTs were fabricated on a heterostructure with a 20 nm n$^+$-InAs cap above an InAlAs/AlSb composite barrier [59]. At NRL, we are investigating structures with a 20 nm n$^+$-InAs cap above an InAlSb barrier [60].

2.6. Microwave and low-frequency noise

As discussed earlier, several groups have now demonstrated low-power InAs HEMTs with values of f_T and f_{max} exceeding 100 GHz. If this technology is to become viable, however, the microwave noise must be low. As shown in Fig. 11, $F_{min} > 1$ dB was measured for frequencies of 2–20 GHz in the first noise measurements reported in 1997 [61]. These relatively large noise figures were caused by the high gate leakage currents. Simulations indicated that a reduction in gate leakage current should result in much lower noise figures (e.g. 0.3 dB at 4 GHz). Devices recently fabricated by Rockwell [43,62] and NGST/NRL [37,63]
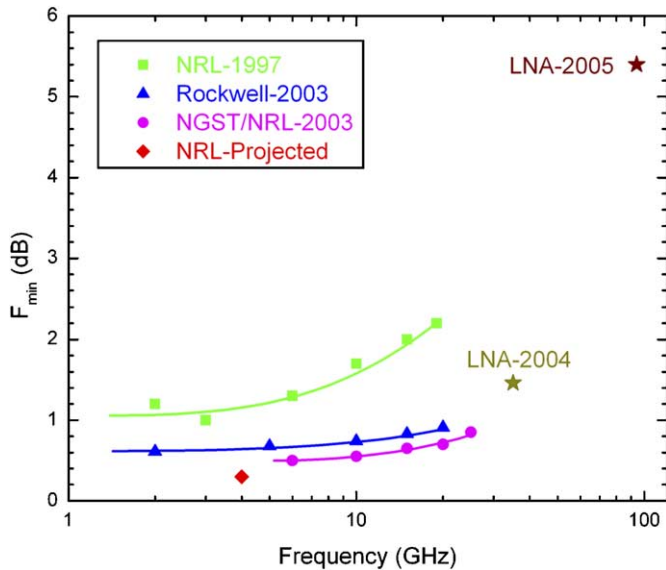
Fig. 11. Noise figure, $F_{\min}$, as a function of frequency for InAs-channel HEMTs [37,61–63,72].

exhibited lower gate leakage current and a substantial reduction in $F_{\min}$, as shown in Fig. 11. These results are very encouraging: they demonstrate that InAs HEMTs have attained microwave noise performance comparable to GaAs- and InP-based HEMTs.

The low-frequency noise of InAs- and InAsSb-channel HEMTs is also of considerable interest for two primary reasons. First, this noise is a very sensitive indicator of material quality, particularly at the interfaces, and therefore can be used to fine-tune material composition and growth parameters. Secondly, since this noise is upconverted in non-linear HEMT circuits, it has a direct bearing on the phase noise of microwave oscillators and phase jitter of high-speed digital circuits. At this time, measurements of the low-frequency noise characteristics of AlSb/InAs/AlSb [64,65] and AlSb/InAsSb/AlSb [66] HEMT structures have been performed. Typical devices whose noise spectra were studied consisted of small HEMT structures, 30 μm wide, with a source–drain length of 3 μm, and gate length of 0.1 μm. The various layer structures examined included InAs channels, digital alloy superlattice channels of InAs/InSb, and random alloy channels of InAsSb. Both undoped and doped devices were included in the study. The measurements were usually done open-channel to avoid gate leakage current whose associated shot noise could affect the results.

Although considerable variations among the noise characteristics were observed, several points can be made to summarize the results of the measurements. The low-frequency noise in the HEMTs consists of the superposition of $1/f$ noise and a local-level component which contributes noise in the temperature range between 150 K and 300 K. An Arrhenius plot of the level yields an activation energy of about 0.38 eV. The value of the Hooge parameter, $\alpha_{\rm H}$, was found to range between 10^{-3} and 10^{-2}. No correlation

between the channel mobility and the Hooge parameter was found in the samples measured. A correlation between the noise and the channel strain, however, was suggested by the results. Specifically, the devices with $InAs_{0.8}Sb_{0.2}$ channels, which are unstrained, had the lowest noise, while those with InAs-channels (in tension) and those with $InAs_{0.7}Sb_{0.3}$ (in compression) were noisier.

It should be noted that no effort has been made at this point to optimize the layer structure, the growth parameters, or the processing procedure in order to minimize the low-frequency noise. Although the Hooge parameter in these devices is about one order of magnitude higher than in the best InP- or GaAs-based HEMTs, the values of $\alpha_{\rm H}$ appear reasonable for a relatively immature technology with a dislocation density of 10^8–10^9 cm^{-2} due to lattice mismatch with respect to the substrate [67,68]. It should also be noted that in all the devices measured at NRL, the noise increases greatly with illumination at low temperatures, and displays a strong Lorentzian spectrum. This noise appears to involve a deep level in the AlSb which can host the photo-excited electrons and thereby also contribute to negative photoconductivity.

2.7. Radiation effects

The low power consumption of InAs HEMTs makes them candidates for applications in space where tolerance to radiation effects is clearly an important issue. Preliminary measurements of laser-induced single-event effect (SEE) characteristics have been performed [69]. The results indicate SEE performance will be similar to that observed previously for InP HEMTs and GaAs FETs under similar excitation conditions. A recent study used proton bombardment to compare the radiation-induced change in drain current for several HEMT material systems [70]. InAs HEMTs were not included in the study, but the conduction band offset between the channel and barrier materials was found to be a key parameter, with larger offsets resulting in smaller changes in drain current. Hence, the 1.35 eV conduction band offset in InAs/AlSb HEMTs should result in excellent tolerance to radiation. Recent experimental results confirm this, with the radiation-induced decrease in HEMT drain currents a factor of 150 lower than for typical GaAs/AlGaAs HEMTs [71].

2.8. Circuits

The first InAs HEMT circuits were reported in 2003–2005. HRL reported an 18-transistor inverter-buffer [39]. The circuit was not designed for depletion-mode devices but the DC transfer curves exhibit the correct functionality. Using a conservative design, NGST/NRL demonstrated an X-band low-noise amplifier (LNA) with greater than 7 dB/stage peak gain between 12 and 14 GHz and 6 mW/stage DC power dissipation [37]. Rockwell fabricated low-power Ka-band LNAs with a noise figure of 1.46 dB at 35 GHz (see Fig. 11) and an associated gain of 22 dB.[72] Most
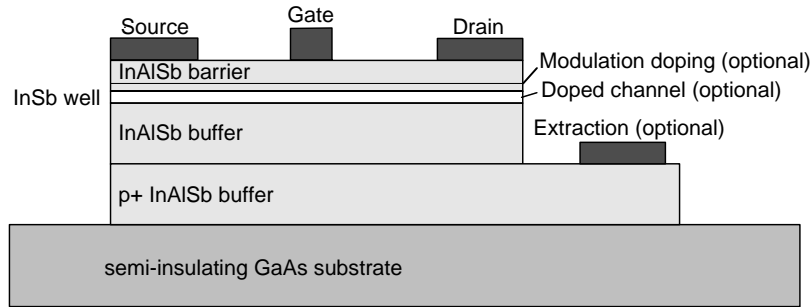
Fig. 12. Cross-section of InSb-channel HEMT with additional contact for carrier extraction [75].

recently, a W-band LNA was reported by NGST/NRL. The 3-stage amplifier has a noise figure of 5.4 dB with an associated gain of 11.1 dB at a total chip dissipation of only 1.8 mW at 94 GHz [63]. The dc power consumption for both the Ka and W-band LNAs was less than one-tenth (one-third) the power for comparable GaAs(InP)-based circuits.

2.9. InSb-channel HEMTs

InSb has a room-temperature electron mobility of 78,000 cm^2/V s, the highest of any semiconductor. In addition, its electron saturation velocity is reported to be greater than 5×10^7 cm/s, compared to 4×10^7 and 1×10^7 cm/s for InAs and GaAs, respectively [73]. In principle, transistors with InSb channels could reach higher frequencies than the InAs-channel HEMTs. Quantum wells can be formed with InSb wells and InAlSb barriers. Room-temperature mobilities as high as 40,000 cm^2/V s have been achieved [74]. The mobility decreases with increasing carrier density, resulting in sheet resistances greater than 200 $\Omega/\square$. The high mobility of InSb should enable low-voltage operation. The high intrinsic carrier concentration ($n_i \sim 10^{16}$/cm^3) and thermal generation rate result in high gate leakage currents. This problem has been mitigated by the use of a carrier extraction technique invented at QinetiQ Corporation [73]. The basic device structure is shown in Fig. 12. The contact to the p^+-InAlSb layer allows the minority carrier density to be reduced by many orders of magnitude. For a gate length of 0.2 μm, an f_T of 150 GHz was achieved at $V_{DS} = 0.5$ V [75].

3. Resonant tunneling diodes

3.1. Background

Resonant tunneling diodes (RTDs) were first fabricated in the GaAs- and InP-based material systems and later in the antimonide system, similar to the situation for HEMTs [76]. In 1988, Luo et al. fabricated RTDs with InAs contact layers, AlSb barriers, and an InAs well [77]. The band diagram is shown in Fig. 13a. Electrons tunnel via conduction band states in the well in this type-I structure. The following year, Söderström et al. reported on the first resonant
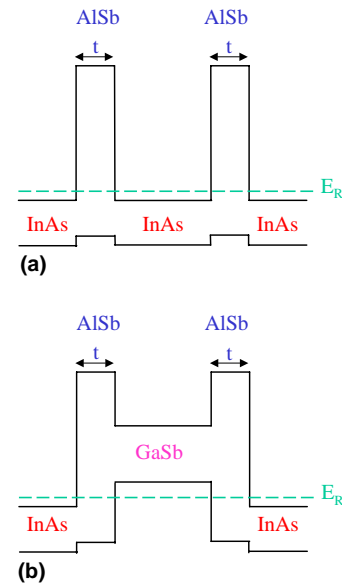
Fig. 13. Conceptual band structure for antimonide-based (a) resonant tunneling diode (RTD) and (b) resonant interband tunneling diode (RITD).

interband tunneling diode (RITD) with the InAs well in the RTD structure replaced by GaSb [78]. As shown in Fig. 13b, the band alignment is type II, with the valence band edge of the GaSb above the conduction band of the InAs. Interband tunneling through the structure occurs when electrons from the InAs conduction band tunnel through the AlSb barrier, into the GaSb valence band, through the second barrier, and into the InAs conduction band. To minimize power dissipation in circuits using resonant tunneling devices it is desirable to have the current peak occur at a low voltage. Schulman's calculations shown in Fig. 14 [79] illustrate the difference between the peak positions of Sb-based RITDs and RTDs. Note that the current peaks at a bias near 100 mV (defined as V_p) for the RITD compared to 200 mV for the RTD. The literature for Sb-based RITDs shows a wide range of V_p values with some as low as 100 mV. The Sb-based RITD peak voltages are also much smaller than the bias voltages of 1–1.5 V that are generally required to reach I_p in GaAs- and InP-based RTDs with the smallest being near 0.4 V [80]. While the RTD and RITD structures in Fig. 13 have

Fig. 14. Calculated *I–V* characteristics for antimonide-based RTDs and RITDs. Note the small bias voltages [79].

been the most often studied structures, the unusual alignment of the valence and conduction bands and the large differences in the bandgaps allow a wide variety of structures to be made. Many of them have been reported in the literature [81–91].
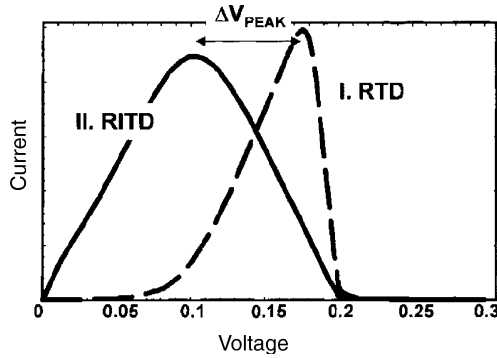
3.2. Performance: peak current density and peak-to-valley ratio

We show typical *I–V* data from one of our RITDs in Fig. 15. The structure was grown on an InAs substrate and was symmetric, consisting of a 1.0 μm InAs ($n \sim 3 \times 10^{18}/cm^3$) buffer layer, 300 Å InAs ($n \sim 1 \times 10^{17}/cm^3$), 120 Å undoped InAs, 15 Å AlSb, 80 Å GaSb, 15 Å AlSb, 120 Å undoped InAs, 300 Å InAs ($n \sim 1 \times 10^{17}/cm^3$), and 0.2 μm InAs ($n \sim 3 \times 10^{18}/cm^3$). The data shown here are for a 3-μm-diameter circular mesa. For positive biases, the figures of merit are: peak current density, $I_p = 1.2 \times 10^4$ A/cm^2 and peak-to-valley ratio (PVR) = 16. For negative biases, $I_p = -1.3 \times 10^4$ A/cm^2 and PVR = 15. Large values of I_p are required for high-speed operation in order to rapidly charge and discharge internal and circuit capa-
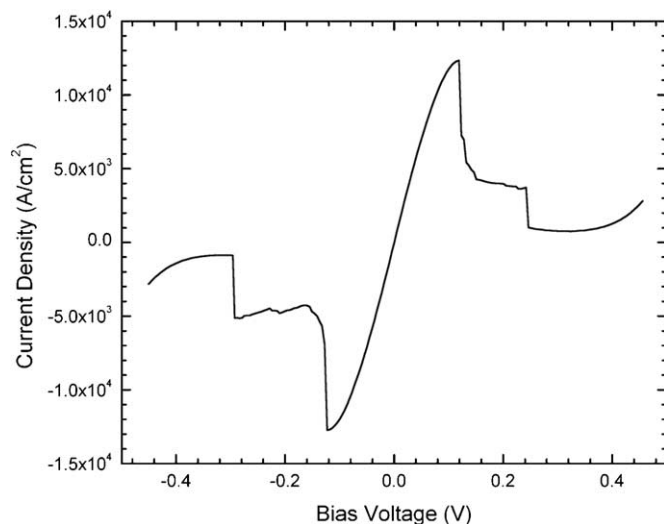

Fig. 15. Current–voltage data for an NRL InAs/AlSb/GaSb/AlSb/InAs RITD with 15 Å barriers.

citances [92,93]. The low valley currents are also desirable for low power dissipation. The peak and valley currents in Fig. 15 are found at the small biases of 120 mV and 300 mV, respectively. This is an important feature of this material system as these low voltages offer the possibility of building low-power-dissipation electronic devices. We have measured devices with peak currents at voltages as low as 65 mV.

Calculating the tunneling current in the InAs/AlSb/GaSb system is very difficult as it requires using at least 8 bands to calculate the wave functions in the various layers for many different values of the in-plane and out-of-plane momentum for each bias. The solution is further complicated by the need to satisfy both the Schrödinger and Poisson equations. In addition to ideal elastic tunneling, the current is determined by a number of phenomena such as phonon interactions [94], interface roughness scattering [95], and impurity scattering [96]. Most of these interactions have been studied in detail in the GaAs/AlGaAs system but not the interband system discussed here.

A starting point for an investigation of resonant interband tunneling is determining the dependence of I_p and the PVR on the barrier thickness. An exponential dependence of I_p on the AlSb barrier thickness is anticipated because the transmission probability for an electron to cross a barrier increases exponentially with decreasing barrier thickness. In Fig. 16a, we plot I_p versus barrier thickness for a set of six samples we grew under nominally identical conditions. Data from other groups is also shown and is in good agreement with our results. The exception is the data point from the first reported RITD; presumably growth procedures were not yet optimized. Fig. 16a indicates that the current increases almost exponentially with decreasing AlSb barrier thickness for thicknesses greater than 10 Å, and somewhat slower for smaller thicknesses. Kitabayashi et al. have reported on the dependence of the tunneling current on the width of the GaSb well and AlSb barrier for barrier widths down to zero [97]. They analyze the difference between the peak current and the valley current and explain their observations in terms of the location of the resonance level in the GaSb well relative to the conduction band edge in the InAs, and the width of the resonance. Their qualitative discussion is based on several assumptions including one that the light-hole band is the dominant band in the GaSb well. They assume that the resonance level moves towards the GaSb valence band edge as the well widens, and that it depends on the barrier thickness. For thin barriers there is a large overlap between the InAs conduction band and GaSb valence band states leading to a smaller effective mass for thin barriers compared to thick barriers. The effective mass contributes to determining the location of the resonance level in the well.

The dependence of the PVR on the barrier thickness has also been examined. In Fig. 16b we show the PVR values corresponding to the data in Fig. 16a and observe a maximum of 20 at an AlSb barrier thickness of 21 Å. There are many possible contributing factors in determining the
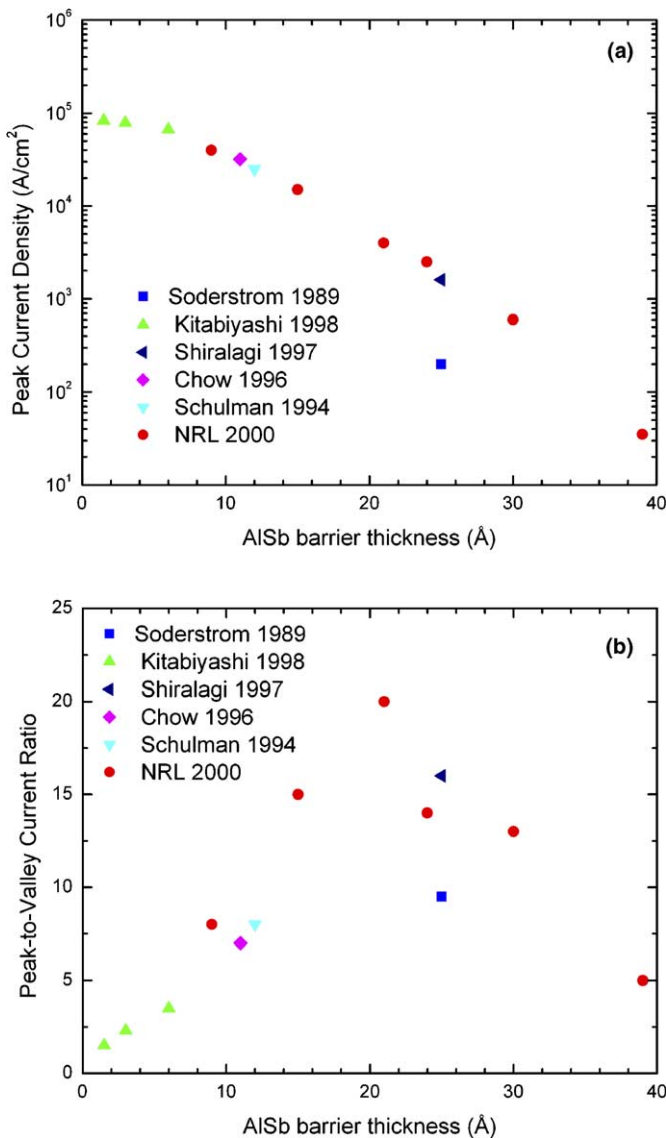
Fig. 16. Peak current density (a) and peak-to-valley ratio (b) as a function of AlSb barrier thickness for symmetric antimonide-based RITDs reported by several groups [78,97,101,102,104,112].

valley current, and the difference in the thickness dependencies of I_p and PVR suggests that different effects dominate at different thickness ranges. Shen measured the temperature dependence of the valley current at several different voltages and proposed that field-assisted thermionic hole emission dominates at room temperature and above, and that Fowler-Nordheim hole tunneling is dominant at low temperature and high fields [98]. More recently, Xu et al. examined the temperature dependence for several devices with barriers from 6 to 20 Å thick [99]. The valley current increased exponentially in all cases but the increase was faster for the thicker barriers. This led to the conclusion that the predominance of thermal emission over hole tunneling increases with increasing barrier thickness. Tehrani et al. reported some success in reducing valley currents by adding a monolayer of AlAs to the barriers to increase the barrier height [100]. This has limited usefulness as it also

reduces the peak current and there is a limit to how thin the barrier can be.

Defects have also been shown to add to the valley current. Shiralagi et al. noted this in a study of the thickness of the InAs buffer needed when using a GaAs substrate to obtain the same PVR as found for an InAs substrate [101]. Magno et al. reported observing features in AFM measurements on RITDs with small PVR that were not present in the topography of diodes with larger PVR [102]. These features are believed to be associated with defects that propagate from the substrate through the RITD layers. RITDs have been exposed to 2 MeV protons in order to study the incremental changes in the peak and valley currents due to defect-assisted processes. Diodes with a thick, 13 ML barrier were more sensitive than those with 5 ML barriers. In both cases the valley current increased faster than the peak current [103].

Ternary alloys have been used in variations of the standard RITD structure shown in Fig. 13 to increase the peak current and PVR. Schulman et al. modified the RITD structure by replacing the GaSb well with $GaAs_xSb_{1-x}$ [104]. The strain should move the heavy-hole band to an energy below the light-hole band. This is expected to reduce the high-bias valley current through the heavy-hole resonance resulting in an improvement in the PVR. Results for several samples with values of x from 0 to 0.3 revealed a maximum PVR = 11 at $x = 0.1$ compared to PVR = 8 at $x = 0$ and PVR = 3 for larger x. Unfortunately, the peak current dropped significantly from a high at $x = 0$. At NRL, we replaced AlSb barriers with AlGaSb and InAlSb in RITD structures. The smaller bandgaps resulted in increases in I_p by as much as a factor of three [105]. PVR values generally decreased for the alloy barriers but remained above 10. An additional advantage of these alloys is that their oxidation rates are substantially lower than pure AlSb which should improve device reliability [38]. The peak current density and PVR for InAs/AlSb RTDs (see Fig. 13a) from several groups are shown in Fig. 17. Compared to the RITDs, higher peak currents have been achieved for antimonide RTDs, with several reports of I_p greater than 1×10^5 A/cm^2 [82,106,107]. The PVRs for the RTDs are smaller than those for the RITDs, and the PVR for the RTD data of Söderström-1990 increases monotonically with thickness unlike the RITD that has a maximum [108]. When an RITD is biased beyond resonance, the electrons must tunnel through the bandgap of the GaSb well in addition to the AlSb barriers. Hence, tunneling contributions to valley currents are minimized, resulting in higher PVRs for RITDs [78].

The values of I_p and PVR for Sb-based RTDs and RITDs are clearly adequate for many potential applications. There have been reports of RTDs using InGaAs alloys for the electrodes and wells along with strained AlAs barriers or unstrained InAlAsSb barriers on InP substrates. PVRs near 50:1 were obtained but with relatively low peak currents of 5.8×10^3 A/cm^2 [109,110]. The peak voltages reported for both these cases were over 750 mV. An
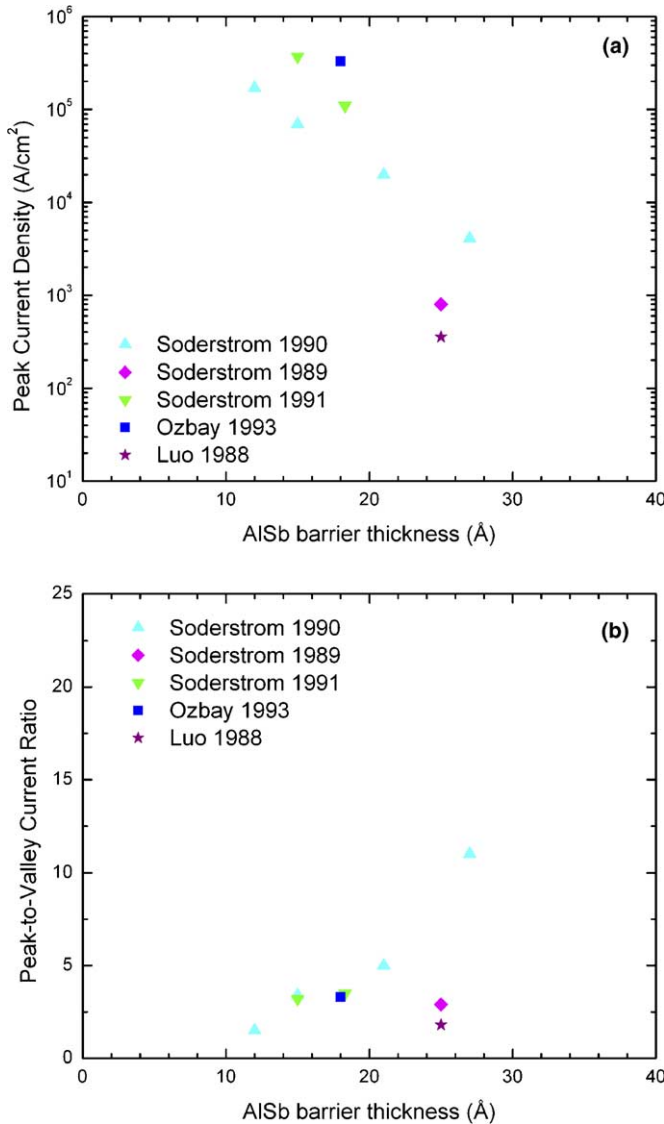
Fig. 17. Peak current density (a) and peak-to-valley ratio (b) as a function of AlSb barrier thickness for symmetric antimonide-based RTDs reported by several groups [77,106–108,113].

Fig. 18. *I–V* characteristics of RITD devices: (a) 3-μm-diameter mesa and (b) 95-μm-diameter mesa. The solid and dashed lines in (b) represent voltage sweeps of different directions, as indicated by arrows [111]. © IEEE.

$I_p = 4.1 \times 10^5$ A/cm^2 has been reported for InP-based RTD with a strained In$_{0.8}$Ga$_{0.2}$As well and strained AlAs barriers. The PVR = 3.8 was reported along with a peak voltage of 680 mV [80].

3.3. Bias voltages and hysteresis

Some care needs to be used in comparing the peak voltages reported in the literature, as all devices will contain some series resistance due to the geometry and quality of the ohmic contacts. The peaks may also be shifted by a voltage drop across depletion regions in the electrodes adjacent to the barriers. The size of the variations in V_p that can result from series resistance effects are illustrated in Fig. 18 [111] by the *I–V* characteristics for RITDs on the same wafer with mesa diameters of 3 μm and 95 μm. Here the small device has $V_p \sim 90$ mV while it is shifted

to ~400 mV for the large device. The peak shift can be understood by recognizing that the applied bias voltage is given by the sum of the voltage drop across the RITD and that across the series resistance. The series resistance is not expected to scale with diode area as there are many contributing factors in addition to mesa diameter. For the 3 μm device, the intrinsic RITD resistance dominates, but for the 95 μm device the series resistance is significant, causing an increase in V_p. This data also illustrates the large hysteresis in the negative resistance region that can result from parasitic series resistance. We have consistently obtained values of V_p near 100 mV for RITDs by using small-diameter mesas with short paths through the InAs to the ohmic contacts as well as short wires to the electronics. Other groups have also reported values near 100 mV [78,97,112]. For Sb-RTDs, values of V_p as low as ~200 mV have been reported [113] while higher values are also found in the literature, presumably due to series resistance effects.

The hysteresis exhibited by the RITD in Fig. 18b is believed to be largely an extrinsic effect since it disappears for the small devices on the same wafer. Hysteresis and peak shifts may be due in part to the storage of charge in the well which is an intrinsic phenomena. Charge storage may also lead to bistabilities that would result in

high-frequency oscillations. Chow and Schulman [114] found that RTDs with AlGaSb barriers and InAs wells and contact layers exhibit an intrinsic bistability. Jimenez et al. also demonstrated intrinsic bistability for RTDs with AlSb barriers and GaSb wells and contact layers [115]. Diode bistability could be useful in the design of high-frequency oscillators and bistable logic circuits.

3.4. Substrates, defects, and interfaces

As discussed in Section 2, there are no suitable semi-insulating substrates with a lattice constant near 6.1 Å. Discrete RTDs and RITDs can be grown on conducting InAs or GaSb substrates, but circuit applications will generally require SI-GaAs or -InP substrates or wafer transfer techniques. Brown et al. compared InAs/AlSb RTDs grown on GaAs and InAs substrates and found little difference in the PVR values, despite the high density of dislocations in the GaAs sample [116]. For RITDs, we have generally found that some of the diodes on GaAs substrates have PVR values equal to devices on InAs substrates, but the uniformity is not as good. AFM imaging reveals that devices which contain a defect have substantially lower PVR values [102]. Shiralagi et al. looked at RITD performance on GaAs substrates as a function of the InAs buffer layer thickness. PVR values increased as the InAs thickness increased, reaching values of 14 for 1 μm buffers, compared to 16 for InAs substrates [101].

If antimonide R(I)TDs are to be used in circuit applications, the uniformity and reproducibility of I_p will be important. State-of-the-art production MBE systems can achieve thickness uniformities of ∼1% across large-diameter substrates. Hence, we do not expect significant variation in I_p as a result of thickness variation across wafers. The presence of defects, especially in the case of lattice-mismatched growth, could be an issue. We have found that defects primarily influence the PVR rather than I_p. In most applications, PVR uniformity will be less important than I_p uniformity. In one case we found that the PVRs across an RITD wafer varied from 18 (no defect) to 9 (defect present) [102]. If, for example, the minimum PVR required for a circuit was 5, then this defect-related non-uniformity would be acceptable. A more serious issue may be run-to-run reproducibility. As mentioned above, I_p is a strong function of AlSb barrier thickness. To obtain high values of I_p ($>1 \times 10^4$ A/cm^2), AlSb barriers less than 15 Å thick are required for RITDs. Hence, variations of 1 Å will cause significant changes in I_p (see Fig. 16a), and the quality of the interfaces is expected to play an important role.

We grew sets of RITDs in which the growth temperature was varied from 350 to 500 °C with other parameters fixed. Remarkably, NDR behavior was observed across this entire range, with values of I_p and I_v varying by less than 20% (for example, the data in Fig. 15 are from a device grown at 350 °C). This suggests that precise control of growth temperature will not be necessary for good reproducibility. The variations that we did observe can be explained by smoother interfaces at higher growth temperatures, resulting in barriers that are effectively thicker, yielding lower I_p values [102].

As discussed in Section 2, either InSb- or AlAs-like bonds can form the interface between InAs and AlSb. Unlike the situation with the HEMTs, however, RITDs can be produced using either bond type [100,101]. In fact, PVR values as high as 30:1 for negative biases were achieved using AlAs interfaces [100]. (These structures were intentionally asymmetric, with much larger PVR but lower I_p for negative biases than for positive bias. Hence, we do not include them in Fig. 16.) Using STM, we found that a quarter monolayer of roughness is introduced at the InAs/AlSb interface due to a change in surface reconstructions when growing InSb interface bonds. This roughness can be eliminated by intentionally depositing 1.25 ML In (rather than 1.0 ML) at the interface [117]. We grew RITDs in which only the InSb-like interface was varied (1.0 and 1.25 ML In). The room-temperature I–V characteristics were very similar. These samples were also characterized by Shubnikov-de Haas oscillations at 1.7 K. The sample with 1.25 ML In showed better-defined oscillations, confirming that the interface was indeed smoother [118].

Some potential applications for antimonide R(I)TDs require very high densities of devices and hence small-diameter diodes. Nomoto et al. fabricated Sb-RTDs with diameters ranging from 100 μm to 20 nm [119,120]. They observed a reduction in PVR for devices smaller than 1 μm and attributed it to a contribution of the surface current to the valley current. Even at 20 nm, NDR behavior was observed. In contrast, the contact layers are pinched off by surface depletion in GaAs RTDs for diameters less than 100 nm [121]. In related work, Shiralagi et al. used epitaxial regrowth on patterned substrates to define sub-micron Sb-RITDs without using any fine-line lithography [122].

3.5. Radiation effects

As mentioned in Section 2, radiation tolerance may be important for Sb-based devices. We reported preliminary measurements for InAs/AlSb/GaSb RITDs [103]. The diodes were able to sustain significant proton irradiation before the I–V characteristics deteriorated. As mentioned earlier, diodes with 5 ML barriers were less sensitive than ones with 13 ML barriers. This is fortunate because the thinner barriers will be required to achieve the large current densities needed for high-frequency operation. Two differences have been noted in the response of an InP-based RTD and an RITD to radiation. The peak current for the InP-based diode decreased with fluence while it increased for the RITD, and an InP-based RTD was more sensitive than the 5-ML-barrier RITD. Additional work is necessary to fully understand these differences. We have also investigated laser-induced single-event effect characteristics [111]. The measurements reveal complex behavior depending on whether the device is biased at a voltage below or above the voltage of the current peak. The

response also occurs with two decay times: a nanosecond and 100 picoseconds for an RITD with a peak current density of 10^3 A/cm^2. A qualitative description based on the different time scales for the decay of electrons and holes stored in the well has been proposed.

3.6. Applications

Several applications for Sb-R(I)TDs have been proposed and demonstrated. Chow and Williamson et al. combined RITDs and Schottky diodes to produce a complete set of logic gates with a maximum operating frequency greater than 12 GHz [112,123]. Shen et al. used RITDs to fabricate static random-access memories and demonstrate bistability and switching [124]. They combined RITDs with InGaAs-channel FETs to demonstrate an exclusive-NOR logic gate [125]. Fay et al. also combined Sb-RITDs with an InGaAs-channel FET and demonstrated an integrated circuit based upon the monostable/bistable logic element (MOBILE) [126]. At NRL, we integrated Sb-RITDs with Sb-HEMTs, as shown in Fig. 19. Both the transistor and diode exhibited good performance (HEMT $f_T = 220$ GHz; RITD $I_p = 1.4 \times 10^4$ A/cm^2 and PVR = 11:1) [127]. Circuits have not been fabricated but modeling suggests that MOBILE circuits with very low power dissipation should be feasible [128]. As discussed in Section 2, Sb-HEMTs exhibit lower power dissipation than InP-based HEMTs, due to operation at lower bias. We have also combined RITDs with giant magnetoresistance elements and demonstrated monostable–bistable transition logic elements [129]. The fast response times were discussed in Section 3.5. Since RITDs with current densities near 10^5 A/cm^2 have been reported, and the frequency scales with current density, RITDs can be expected to operate at frequencies above

100 GHz. In a landmark study, Brown et al. reported an InAs/AlSb RTD operating at 712 GHz [130].

The final application we will discuss in this section is the mm-wave backward diode. The basic structure consists of a single AlSb barrier, separating n-InAs and p-GaSb, as shown in Fig. 20a. Luo et al. [131] and Chen et al. [132] demonstrated negative resistance from this structure. Schulman and co-workers applied these diodes to mm-wave detection, translating low-level rf power into dc
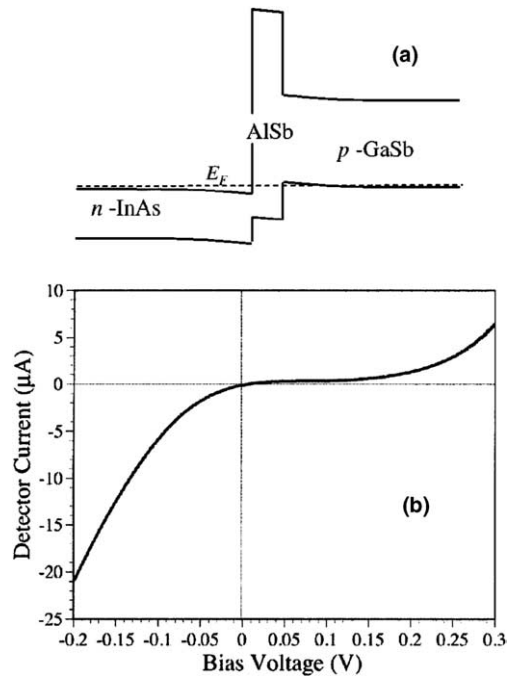

Fig. 20. Band diagram and *I–V* characteristics from HRL backward-diode for mm-wave detection [133,134]. © IEEE.
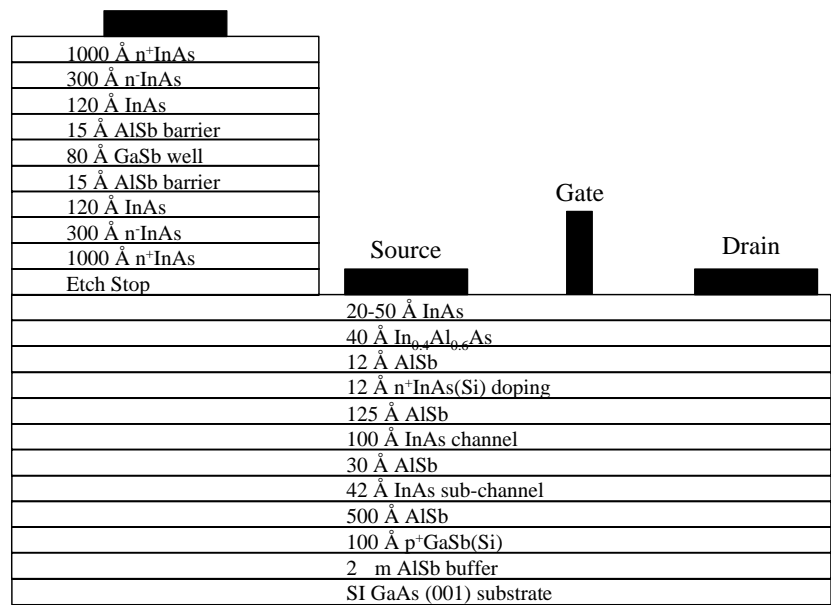

Fig. 19. Cross-section for antimonide-based RITD and HEMT grown in a single heterostructure at NRL [127]. © 2000, AVS The Science and Technology Society.

voltage or current with extreme linearity and low noise [133–135]. In Fig. 20b, we show their *I–V* characteristic for a $1.5 \times 1.5\ \mu m^2$ detector. The large curvature at zero bias translates into good responsivity at a frequency of 95 GHz. Unlike other Sb-based devices discussed in this review, the mm-wave detector is already used in a commercial product.

4. Heterojunction bipolar transistors

4.1. Background and early work

The design and growth of an HBT is generally more challenging than a HEMT or R(I)TD because of the need to obtain the appropriate conduction- and valence-band offsets at the emitter–base and base–collector heterojunctions. High current gains require low carrier recombination rates in the base and at the emitter–base junction, thus low defect concentrations are desirable. High mobilities are desirable to minimize the transit time across the base and collector depletion regions, enabling high-frequency operation. High mobilities and low resistance ohmic contacts also help to minimize parasitic resistances that slow devices through large RC time constants. High-frequency operation requires large collector currents. Hence, power dissipation becomes a problem that can be handled by using high-thermal-conductivity materials and devices that operate at low voltage. To attain high performance requires making wise choices particularly in the choice of materials given that optimum device geometry may be obtained in any material system. These facts, combined with the relative immaturity of the antimonide-based materials systems, resulted in relatively little work on antimonide-based/narrow-bandgap HBTs until recently. This system has advantages in that materials such as InAs and InGaSb have narrow bandgaps and high electron and hole mobilities that make them attractive for use as the base. The small bandgaps should lead to low power dissipation through use of small emitter–base and emitter–collector voltages, and the high mobilities should lead to high-frequency operation. The choice of semiconductors for the emitter and collector with suitable bandgaps and band offsets becomes a major consideration. They should be closely lattice matched to the base, and have a large valence band offset relative to the base. While there is data in the literature on the bandgaps and band offsets of some of the relevant materials there are many uncertainties in the details. There are a number of publications listing interpolation routines and bowing parameter data that are useful as a starting point. The lack of a commercial semi-insulating substrate with a lattice constant near that of InAs and GaSb is another difficulty.

Vergurlekar et al. published their results on the development of a hot-electron AlSb/InAs bipolar transistor in 1990. They showed that the large conduction band discontinuity between InAs and AlSb resulted in impact ionization when electrons were injected into a p-InAs base

across the AlSb/InAs heterojunction [136]. Two years later, Pekarik et al. demonstrated the first AlSb–InAs–AlSb pnp HBT. The devices exhibited current gain but were limited by extremely large base currents, apparently due to extensive interface recombination [137]. Dodd et al. fabricated npn InAs bipolar transistors on InP in an attempt to achieve pseudo-HBT performance due to bandgap narrowing. Current gains of 30 were achieved at room temperature but junction leakage currents were very high. The dc performance was improved when the structure was grown on an InAs substrate [138]. Transistors grown on a conductive substrate, however, cannot be used at microwave frequencies. For this reason, Moran et al. used wafer bonding to transfer an antimonide-based npn HBT from a GaSb substrate to an insulating sapphire substrate [139]. The transistors exhibited a dc current gain of 5.

4.2. HBTs with InAs and InGaAs bases

One approach to narrow-gap HBTs is to use InAs as the base with alloys as the emitter and/or collector. Averett and co-workers fabricated npn HBTs with an InAs base and collector and InAlAs or InAsP emitters [140–142]. Thomas et al. at HRL used InAsP as both the emitter and collector [143]. In Fig. 21, we plot the collector current density, J_C, as a function of the emitter–base voltage, V_{BE}, for several materials systems [144,145]. As expected, as the bandgap of the base decreases, the emitter–base voltage for a given collector current also decreases. The HRL devices demonstrated low-power operation, with gain for V_{BE} between 0.1 and 0.3 V. When transferred to a sapphire substrate, the HBTs exhibited excellent microwave performance with an f_T of 181 GHz. Divide-by-16 circuits consisting of 62 transistors were demonstrated and exhibited a maximum operating frequency of 10 GHz [143].

Conventional HBTs lattice-matched to SI-InP substrates use $In_{0.53}Ga_{0.47}As$ as the base with either InP or $In_{0.52}Al_{0.48}As$ for the emitter and InP or $In_{0.53}Ga_{0.47}As$ as the collector. A narrow-gap alternative is to use InAlAs
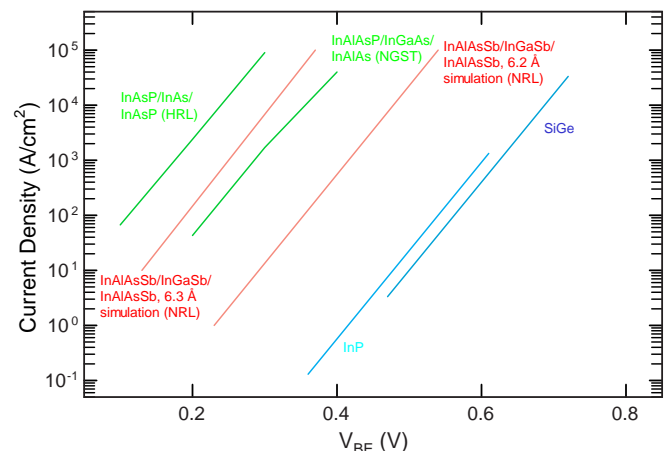

Fig. 21. Collector current density versus base-emitter voltage for npn HBTs [143–146,149].

and InGaAs with indium concentrations greater than 80% in all three layers. Monier et al. at NGST demonstrated npn HBTs using an $In_{0.86}Al_{0.14}As/In_{0.86}Ga_{0.14}As/In_{0.86}Al_{0.14}As$ structure with a 6.0 Å lattice constant [146]. The devices were grown on InP substrates using graded InAlAs buffer layers [147]. Gain was achieved with V_{BE} between 0.2 and 0.4 V, as shown in Fig. 21. Microwave measurements yielded a peak cut-off frequency of 170 GHz. Initial test circuits include 28 GHz dividers that dissipate half the power of InP-based circuits [148].

4.3. InGaSb/InAlAsSb npn HBTs

At NRL, we surveyed materials and band offsets and selected a material system with a lattice constant near 6.2 Å [149]. The willingness to try working with a large lattice mismatch was motivated in part by the success in the InP community in developing metamorphic growth techniques allowing the use of GaAs substrates in the growth of HBTs and HEMTs lattice matched to InP. Past success at NRL in growing InAs/AlSb HEMTs on GaAs also was considered. For developmental purposes commercial GaSb substrates were chosen to minimize the lattice mismatch rather than the preferred semi-insulating GaAs or InP. $In_xGa_{1-x}Sb$ was chosen for the base because of its small bandgap and to exploit the good hole transport characteristics of these alloys. In addition, low-resistance ohmic contacts to p-InGaSb have been achieved [150–152]. These properties are important factors in minimizing the base resistance. Equally important is the fact that a narrow bandgap InGaSb base can be used with a collector and an emitter made from a variety of InAlAsSb alloys. While little is known about the details of the band offsets and bandgaps of these materials, extrapolations from known binary and ternary alloys indicate that it should be possible to have a large valence band offset of 300 mV or more over a wide range of InAlAsSb alloys, particularly with alloys having a 6.2 Å lattice constant [3]. This is important in minimizing the parasitic hole current flow from the InGaSb base to the emitter. The InAlAsSb alloys are predicted to be direct bandgap semiconductors over a range of bandgaps from 0.2 to 1.4 eV. This leads to a wide range of possible conduction band offsets with the InGaSb base because the valence band offset is almost insensitive to the InAlAsSb composition. The above listed properties allow a great deal of latitude in using band-structure engineering to optimize HBT performance. One possible emitter–base–collector structure with estimated band offsets is illustrated in Fig. 22. The negative side to using InAlAsSb alloys with the desired composition is that they are expected to be hard to grow as controlling the As/Sb composition is difficult, and there may be miscibility gap problems. Methods for obtaining n-type doping also are required.

The structure in Fig. 22 was grown on an undoped GaSb substrate with a 1 μm AlSb buffer layer [153]. The collector was 1 μm thick with a nominal $n = 3 \times 10^{16}/cm^3$ doping; the base was 0.1 μm thick with a nominal $p = 5 \times 10^{18}/cm^3$
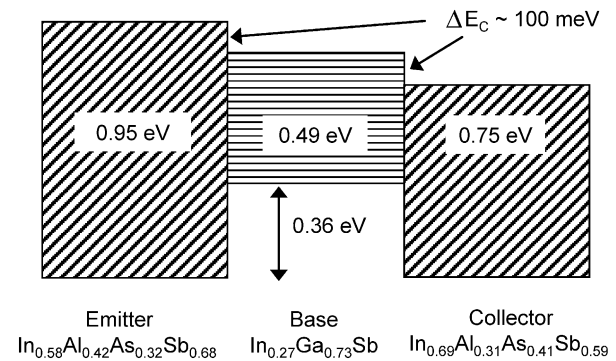

Fig. 22. Predicted band diagram for InAlAsSb/InGaSb/InAlAsSb npn HBT with $a_o = 6.20$ Å [149].

doping; the emitter was 0.2 μm thick with a nominal $n = 3 \times 10^{17}/cm^3$ doping. The heterostructure also included a heavily doped 0.1 μm layer grown between the collector and the AlSb buffer. This layer has the same composition as the collector and it was included to improve the electrical contact to the collector. Heavily doped contact layers have been used on the top of the emitter to aid in contacting it. Rather conservative layer designs were used in this structure. A relatively low base doping was chosen to avoid possible problems associated with Be segregating into the emitter. A thick base was used to make it easier to etch down to it using an iterative etch test procedure. A thick collector was used to accommodate the lattice mismatch between the AlSb with a 6.136 Å lattice constant and the 6.2 Å HBT structure. A variety of emitter shapes were fabricated with relatively large areas of 30–60 μm².

The common emitter curves for the layer structure in Fig. 22 are shown in Fig. 23. It has a DC current gain of 25 and has been measured to $V_{CE} = 5$ V without damage to the device. The maximum collector current, I_C, in Fig. 23 corresponds to a density of 1.8×10^4 A/cm². The low collector–emitter offset voltage of 220 mV supports the possibility of low power dissipation. Current–voltage measurements on the emitter–base and collector-base p-n junctions indicate that series resistances are spreading the voltage over which I_C increases from zero in Fig. 23. Much higher collector currents densities are expected at lower base-emitter voltages for the InGaSb devices compared to
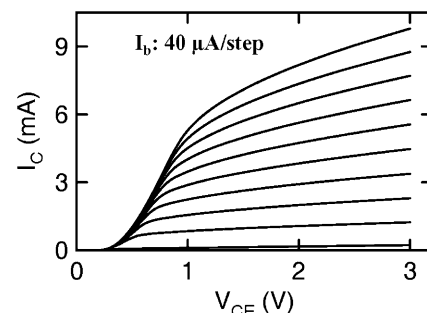

Fig. 23. *I–V* characteristics from InAlAsSb/InGaSb/InAlAsSb npn HBT [153]. © IEE.
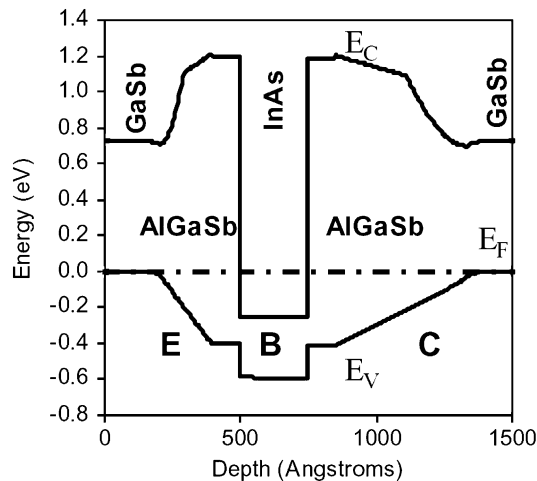
Fig. 24. Band diagram for pnp HBT demonstrated by Rockwell [154]. © IEEE.

conventional InP or SiGe HBTs. This is important because large collector currents are required for high-frequency operation, and small values of V_{BE} indicate that low power dissipation is possible.

4.4. pnp Structures and InP HBTs with GaAsSb bases

With the exception of the 1992 paper by Pekarik et al., all the above work involves npn structures. Recently, Rockwell demonstrated a pnp structure with an InAs base and AlGaSb emitter and collector [154]. The bandstructure is shown in Fig. 24. The device exhibits gain for base-emitter voltages as low as 0.2 V.

Our discussion here has focused on HBTs with very narrow bandgaps and large lattice constants (6.0–6.2 Å), regardless of whether the heterostructures included Sb. There has been an important advance involving the use of Sb in InP-based HBTs. Specifically, the $In_{0.53}Ga_{0.47}As$ base can be replaced with $GaAs_{0.51}Sb_{0.49}$ to give a type-II band alignment to reduce collector-current blocking. Excellent HBT performance has been achieved with these structures [155–157].

5. Summary and outlook

In this paper, we have reviewed the recent progress on three antimonide-based electronic devices: HEMTs, R(I)TDs, and HBTs. For all three devices, the advantage of Sb-based structures over Si-, GaAs-, or InP-based structures is the attainment of high-frequency operation with much lower power consumption. For the HEMT, recent advances include the demonstration of Ka- and W-band LNA circuits that operate at less than one-third the power of similar InP-based circuits. Applications may also include low-power logic; advantages and obstacles are discussed in a recent article [158]. Active areas of HEMT research include reduction of the gate-to-channel spacing for sub-100-nm gate length and reduction of gate leakage currents.

The R(I)TDs have been heavily studied and considered for application in MOBILE circuits, but, like their InP- and GaAs-based counterparts, are waiting for a viable commercial application. Spintronic concepts using RITDs both with and without ferromagnetic semiconductor materials have also been reported [159–163]. Several groups have been investigating HBTs based upon narrow-bandgap materials in the last three years. Most approaches involve lattice constants of 6.0–6.1 Å with InAs or $In_{0.86}Ga_{0.14}As$ as the base and InAs or related alloys such as InAsP or InAlAs as the emitter and collector. Divider circuits have been reported. An alternative approach is to work at a 6.2–6.3 Å lattice constant using InGaSb as the base and InAlAsSb alloys as the emitter and collector.

Future systems could also include unconventional devices that take advantage of the properties of antimonides. A good example of this is the backward diode being developed for use in THz imaging [133]. THz source concepts using these materials have also been suggested and need to be examined [164]. The large conduction band offsets between AlSb and InAs and the large electron mobility in InAs make this system useful in the fabrication of one-dimensional quantum wires. Advances in the lateral patterning by C.H. Yang and colleagues have allowed them to demonstrate low-temperature electron elastic mean free paths greater than 1.4 μm and coherence lengths greater than 3 μm [165]. Such structures could form the basis of future electronic devices.

Antimonide-based electronics may also benefit from growth and processing advances resulting from work on electro-optic devices. The wide variety of bandgaps and offsets along with the high mobilities are being exploited to develop long-wavelength (8–25 μm) superlattice detectors that are predicted to have superior performance to the HgCdTe detectors [166]. Lasers emitting in the 2–5 μm range are also being developed [167].

As we have discussed, there has been considerable progress in Sb-based electronic devices in the last few years. The advances are especially significant considering the relatively low level of funding and effort, compared, for example, to InP-based electronics in the 1980s. In our view, it is unrealistic to think that Sb-based electronics will replace a large fraction of GaAs- or InP-based devices. However, they are promising for specific applications where both high-frequency operation and low power consumption are needed. System applications that have already transitioned from GaAs- to InP-electronics to achieve lower power consumption may be candidates for transition to antimonides.

Acknowledgements

R. Bass, A.S. Bracker, P.M. Campbell, J.C. Culbertson, E.R. Glaser, M. Goldenberg, K.D. Hobart, D. McMorrow, N. Papanicolaou, D. Park, B.V. Shanabrook, B.P. Tinkham, R.J. Wagner, B.D. Weaver, and M.J. Yang; and collaborators at Northrop Grumman Corporation: W.R. Deal, A. Gutierrez, M.D. Lange, and R. Tsai.

References

[1] Nguyen LD, Larson LE, Mishra UK. Ultra-high-speed modulation-doped field-effect transistors—a tutorial review. Proc IEEE 1992; 80(4):494–518.

[2] Dobrovolskis Z, Grigoras K, Krotkus A. Measurement of the hot-electron conductivity in semiconductors using ultrafast electric pulses. Appl Phys A-Mater 1989;48(3):245–9.

[3] Vurgaftman I, Meyer JR, Ram-Mohan LR. Band parameters for III–V compound semiconductors and their alloys. J Appl Phys 2001; 89(11):5815–75.

[4] Milnes AG, Polyakov AY. Indium arsenide—a semiconductor for high-speed and electrooptical devices. Mater Sci Eng B-Solid 1993; 18(3):237–59.

[5] Milnes AG, Polyakov AY. Gallium antimonide device related properties. Solid-State Electron 1993;36(6):803–18.

[6] Dutta PS, Bhat HL, Kumar V. The physics and technology of gallium antimonide: an emerging optoelectronic material. J Appl Phys 1997;81(9):5821–70.

[7] Chang CA, Ludeke R, Chang LL, Esaki L. Molecular-beam epitaxy (MBE) of InGaAs and GaSbAs. Appl Phys Lett 1977;31(11):759–61.

[8] Yano M, Suzuki Y, Ishii T, Matsushima Y, Kimata M. Molecular-beam epitaxy of GaSb and GaSbAs. Jpn J Appl Phys 1978;17(12): 2091–6.

[9] Ludeke R. Electronic properties of (100) surfaces of GaSb and InAs and their alloys with GaAs. IBM J Res Dev 1978;22(3):304–14.

[10] Bennett BR, Shanabrook BV. Molecular beam epitaxy of Sb-based semiconductors. In: Liu AWK, Santos MB, editors. Thin films: heteroepitaxial systems. Singapore: World Scientific; 1999. p. 401–52.

[11] Tuttle G, Kroemer H, English JH. Electron concentrations and mobilities in AlSb/InAs/AlSb quantum wells. J Appl Phys 1989; 65(12):5239–42.

[12] Tuttle G, Kroemer H, English JH. Effects of interface layer sequencing on the transport-properties of InAs/AlSb quantum-wells—evidence for antisite donors at the InAs/AlSb interface. J Appl Phys 1990;67(6):3032–7.

[13] Bolognesi CR, Kroemer H, English JH. Well width dependence of electron-transport in molecular-beam epitaxially grown InAs/AlSb quantum-wells. J Vac Sci Technol B 1992;10(2):877–9.

[14] Koester SJ, Bolognesi CR, Thomas M, Hu EL, Kroemer H, Rooks MJ. Determination of one-dimensional subband spacings in InAs/ AlSb ballistic constrictions using magnetic-field measurements. Phys Rev B 1994;50(8):5710–2.

[15] Yang CH, Yang MJ, Cheng KA, Culbertson JC. Characterization of one-dimensional quantum channels in InAs/AlSb. Phys Rev B 2002;66(11):115306.

[16] Kuze N, Nagase K, Muramatsu S, Miya S, Iwabuchi T, Ichii A, et al. InAs deep quantum-well structures and their application to hall elements. J Cryst Growth 1995;150(1–4):1307–12.

[17] Behet M, Nemeth S, De Boeck J, Borghs G, Tummler J, Woitok J, et al. Molecular beam epitaxy and characterization of InAs/AlGaSb heterostructures for magnetic sensing applications. Semicond Sci Technol 1998;13(4):428–32.

[18] Johnson M, Bennett BR, Yang MJ, Miller MM, Shanabrook BV. Hybrid hall effect device. Appl Phys Lett 1997;71(7):974–6.

[19] Johnson M, Bennett BR, Hammar PR, Miller MM. Magnetoelectronic latching Boolean gate. Solid-State Electron 2000;44(6): 1099–104.

[20] Nguyen C, Brar B, Kroemer H. Surface-layer modulation of electron concentrations in InAs–AlSb quantum-wells. J Vac Sci Technol B 1993;11(4):1706–9.

[21] Boos JB, Kruppa W, Bennett BR, Park D, Kirchoefer SW, Bass R, et al. AlSb/InAs HEMT's for low-voltage, high-speed applications. IEEE Trans Electron Dev 1998;45(9):1869–75.

[22] Venkatasubramanian R, Dorsey DL, Mahalingam K. Heuristic rules for group IV dopant site selection in III–V compounds. J Cryst Growth 1997;175:224–8.

[23] Sasa S, Yamamoto Y, Izumiya S, Yano M, Iwai Y, Inoue M. Increased electron concentration in InAs/AlGaSb heterostructures using a Si planar doped ultrathin InAs quantum well. Jpn J Appl Phys 1 1997;36(3B):1869–71.

[24] Zhao Y, Jurkovic MJ, Wang WI. Kink-free characteristics of AlSb/ InAs high electron mobility transistors with planar Si doping beneath the channel. IEEE Trans Electron Dev 1998;45(1):341–2.

[25] Bolognesi CR, Dvorak MW, Chow DH. High-transconductance delta-doped InAs/AlSb HFET's with ultrathin silicon-doped InAs quantum well donor layer. IEEE Electron Dev Lett 1998;19(3):83–5.

[26] Bennett BR, Yang MJ, Shanabrook BV, Boos JB, Park D. Modulation doping of InAs/AlSb quantum wells using remote InAs donor layers. Appl Phys Lett 1998;72(10):1193–5.

[27] Bolognesi CR, Bryce JE, Chow DH. InAs channel heterostructure-field effect transistors with InAs/AISb short-period superlattice barriers. Appl Phys Lett 1996;69(23):3531–3.

[28] Furukawa A, Mizuta M. Heterojunction bipolar-transistor utilizing AlGaSb/GaSb alloy system. Electron Lett 1988;24(22):1378–80.

[29] Wood CEC. Surface exchange doping of MBE GaAs from S and Se captive sources. Appl Phys Lett 1978;33(8):770–2.

[30] Subbanna S, Tuttle G, Kroemer H. N-type doping of gallium antimonide and aluminum antimonide grown by molecular-beam epitaxy using lead-telluride as a tellurium dopant source. J Electron Mater 1988;17(4):297–303.

[31] Turner GW, Eglash SJ, Strauss AJ. Molecular-beam epitaxial-growth of high-mobility n-GaSb. J Vac Sci Technol B 1993;11(3): 864–7.

[32] Bennett BR, Magno R, Papanicolaou N. Controlled n-type doping of antimonides and arsenides using GaTe. J Cryst Growth 2003; 251(1–4):532–7.

[33] Bergman J, Nagy G, Sullivan G, Brar B, Kadow C, Lin H-K, et al. InAs/AlSb HFETs with f_T and f_{max} above 150 GHz for low-power MMICs. In: Proc InP related mater conf, 2003. p. 219–22.

[34] Nguyen C, Ensslin K, Kroemer H. Magnetotransport in InAs/AlSb quantum-wells with large electron-concentration modulation. Surf Sci 1992;267(1–3):549–52.

[35] Bennett BR, Tinkham BP, Boos JB, Lange MD, Tsai R. Materials growth for InAs high electron mobility transistors and circuits. J Vac Sci Technol B 2004;22(2):688–94.

[36] Bolognesi CR, Caine EJ, Kroemer H. Improved charge control and frequency performance in InAs/AlSb-based heterostructure field-effect transistors. IEEE Electron Dev Lett 1994;15(1):16–8.

[37] Tsai R, Barsky M, Boos JB, Bennett BR, Lee J, Papanicolaou NA, et al. Metamorphic AlSb/InAs HEMT for low-power, high-speed electronics. In: Proc IEEE GaAs IC symp, 2003. p. 294–7.

[38] Miya S, Muramatsu S, Kuze N, Nagase K, Iwabuchi T, Ichii A, et al. AlGaAsSb buffer barrier on GaAs substrate for InAs channel devices with high electron mobility and practical reliability. J Electron Mater 1996;25(3):415–20.

[39] Royter Y, Elliott KR, Deelman PW, Rajavel RD, Chow DH, Milosavljevic I, et al. High frequency InAs-channel HEMTs for low power ICs. Tech Digest IEDM 2003:30.7.1–4.

[40] Boos JB, Bennett BR, Kruppa W, Park D, Mittereder J, Bass R, et al. Ohmic contacts in AlSb InAs high electron mobility transistors for low-voltage operation. J Vac Sci Technol B 1999;17(3): 1022–7.

[41] Tsai R, Boos JB, Bennett BR, Lange MD, Grundbacker R, Namba C, et al. 275 GHz f_{max}, 220 GHz f_T AlSb/InAs HEMT technology. In: Dev res conf, 2004. p. 2: 12–3.

[42] Tsai R, Grundbacker R, Lange MD, Boos JB, Bennett BR, Nam P, et al. Manufacturable AlSb/InAs HEMT technology for ultra-low power millimeter-wave integrated circuits. In: GaAs mantech conf, 2004. p. 4.

[43] Bergman J, Nagy G, Sullivan G, Ikhlassi A, Brar B, Kadow C, et al. Low-voltage, high-performance InAs/AlSb HEMTs with power gain above 100 GHz at 100 mV drain bias. In: Dev res conf, 2004. p. 243–4.

[44] Yang MJ, Wang FC, Yang CH, Bennett BR, Do TQ. A composite quantum well field-effect transistor. Appl Phys Lett 1996;69(1):85–7.

[45] Boos JB, Yang MJ, Bennett BR, Park D, Kruppa W, Yang CH, et al. 0.1 μm AlSb/InAs HEMTs with InAs subchannel. Electron Lett 1998;34(15):1525–6.

[46] Lin HK, Kadow C, Dahlstrom M, Bae JU, Rodwell MJW, Gossard AC, et al. InAs/InAsP composite channels for antimonide-based field-effect transistors. Appl Phys Lett 2004;84(3):437–9.

[47] Lin HK, Kadow C, Bae JU, Rodwell MJW, Gossard AC, Brar B, et al. Design and characteristics of strained InAs/InAlAs composite-channel heterostructure field-effect transistors. J Appl Phys 2005;97(2):024505.

[48] Yang MJ, Bennett BR, Fatemi M, Lin-Chung PJ, Moore WJ, Yang CH. Photoluminescence of InAsSb/AlSb single quantum wells: transition from type-II to type-I band alignment. J Appl Phys 2000;87(11):8192–4.

[49] Boos JB, Yang MJ, Bennett BR, Park D, Kruppa W, Bass R. Low-voltage, high-speed AlSb InAsSb HEMTs. Electron Lett 1999;35(10):847–8.

[50] Papanicolaou N, Tinkham BP, Boos JB, Bennett BR, Bass R, Park D. 6.2 Å $In_{0.2}Al_{0.8}Sb/InAs_{0.7}Sb_{0.3}$ HEMTs for low-voltage high-frequency applications. In: Intl semicon dev res symp, 2003.

[51] Tinkham BP, Bennett BR, Magno R, Shanabrook BV, Boos JB. Growth of InAsSb-channel high electron mobility transistor structures. J Vac Sci Technol B 2005;23(4):1441–4.

[52] Brar B, Kroemer H. Influence of impact ionization on the drain conductance in InAs–AlSb quantum-well heterostructure field-effect transistors. IEEE Electron Dev Lett 1995;16(12):548–50.

[53] Longenbach KF, Beresford R, Wang WI. Application of split-gate and dual-gate field-effect transistor designs to InAs field-effect transistors. Solid-State Electron 1990;33(9):1211–3.

[54] Boos JB, Kruppa W, Park D. Reduction of gate current in AlSb/InAs HEMTs using a dual-gate design. Electron Lett 1996;32(17):1624–5.

[55] Bolognesi CR, Chow DH. InAs/AlSb dual-gate HFET's. IEEE Electron Dev Lett 1996;17(11):534–6.

[56] Zhao Y, Jurkovic MJ, Wang WI. Enhancement-mode InAs n-channel high electron mobility transistors using Beryllium sheet doping. Solid-State Electron 1998;42(1):57–61.

[57] Kadow C, Lin HK, Dahlstrom M, Rodwell M, Gossard AC, Brar B, et al. Reduction of the unintentional background electron density in AlSb/InAs/AlSb quantum wells. J Cryst Growth 2003;251(1–4):543–6.

[58] Triplett GE, Brown AS, May GS. Charge modification in InAs/AlGaSb HEMT structures. J Cryst Growth 2004;265(1–2):47–52.

[59] Kadow C, Dahlstrom M, Bae JU, Lin HK, Gossard AC, Rodwell MJW, et al. n(+)-InAs–InAlAs recess gate technology for InAs-channel millimeter-wave HFETs. IEEE Trans Electron Dev 2005;52(2):151–8.

[60] Bennett BR, Boos JB, Ancona MG, Papanicolaou N, Park D, Bass R. InAs quantum well heterostructures for FETs with ultra-short gates. In: Electron mater conf, 2005.

[61] Kruppa W, Boos JB, Park D, Bennett BR, Bass R. Microwave noise characteristics of AlSb/InAs HEMTs. Electron Lett 1997;33(12):1092–3.

[62] Bergman J, Nagy G, Sullivan G, Brar B, Kadow C, Lin H-K, et al. RF noise performance of low power InAs/AlSb HFETs. In: Proc dev res conf, 2003. p. 147–8.

[63] Deal WR, Tsai R, Lange MD, Boos JB, Bennett BR, Gutierrez A. A W-band InAs/AlSb low-noise/low-power amplifier. IEEE Microw Wirel Co 2005;15(4):208–10.

[64] Kruppa W, Boos JB, Bennett BR, Yang MJ. Low-frequency noise in AlSb/InAs HEMTs. Electron Lett 2000;36(22):1888–9.

[65] Kruppa W, Yang MJ, Bennett BR, Boos JB. Low-frequency noise in AlSb/InAs high-electron-mobility transistor structure as a function of temperature and illumination. Appl Phys Lett 2004;85(5):774–6.

[66] Kruppa W, Boos JB, Bennett BR, Tinkham BP. Low-frequency noise characteristics of AlSb/InAsSb HEMTs. Solid-State Electron 2004;48(10–11):2079–84.

[67] Spitzer J, Hopner A, Kuball M, Cardona M, Jenichen B, Neuroth H, et al. Influence of the interlace composition of InAs/AlSb superlattices on their optical and structural-properties. J Appl Phys 1995;77(2):811–20.

[68] Kramer GD, Adam MS, Tsui RK, Theodore ND. Characterization of dislocation reduction in MBE-grown (Al, Ga)Sb/GaAs by TEM. In: Gallium arsenide and related compounds, 1994. p. 727–32.

[69] McMorrow D, Boos JB, Knudson AR, Buchner S, Yang MJ, Bennett BR, et al. Charge-collection characteristics of low-power ultrahigh speed, metamorphic AlSb/InAs high-electron mobility transistors (HEMTs). IEEE Trans Nucl Sci 2000;47(6):2662–8.

[70] Weaver BD, Jackson EM. Universal behavior in irradiated high-electron-mobility transistors. Appl Phys Lett 2002;80(15):2791–3.

[71] Weaver BD, Boos JB, Papanicolau NA, Bennett BR, Park D, Bass R. High radiation tolerance of InAs/AlSb high electron mobility transistors. Appl Phys Lett 2005;87:173501.

[72] Hacker JB, Bergman J, Nagy G, Sullivan G, Kadow C, Lin HK, et al. An ultra-low power InAs/AlSb HEMT Ka-band low-noise amplifier. IEEE Microw Wirel Co 2004;14(4):156–8.

[73] Ashley T, Dean AB, Elliott CT, Pryce GJ, Johnson AD, Willis H. Uncooled high-speed InSb field-effect transistors. Appl Phys Lett 1995;66(4):481–3.

[74] Goldammer KJ, Chung SJ, Liu WK, Santos MB, Hicks JL, Raymond S, et al. High-mobility electron systems in remotely-doped InSb quantum wells. J Cryst Growth 1999;202:753–6.

[75] Ashley T. Novel InSb-based quantum well transistors for ultra-high speed, low power logic applications. In: Intl conf sol state & IC technol, 2004.

[76] Sun JP, Haddad GI, Mazumder P, Schulman JN. Resonant tunneling diodes: models and properties. Proc IEEE 1998;86(4):641–61.

[77] Luo LF, Beresford R, Wang WI. Resonant tunneling in AlSb/InAs/AlSb double-barrier heterostructures. Appl Phys Lett 1988;53(23):2320–2.

[78] Soderstrom JR, Chow DH, Mcgill TC. New negative differential resistance device based on resonant interband tunneling. Appl Phys Lett 1989;55(11):1094–6.

[79] Schulman JN. Analysis of Sb-based resonant interband tunnel diodes for circuit modeling. Solid-State Electron 1999;43(8):1367–71.

[80] Sugiyama H, Matsuzaki H, Oda Y, Yokoyama H, Enoki T, Kobayashi T. InP-based strained InGaAs/AlAs resonant tunneling diodes with high peak-current density and large peak-to-valley current ratio grown by metal-organic vapor-phase epitaxy. In: Proc InP and related mater conf, 2003. p. 211–4.

[81] Soderstrom JR, Chow DH, Mcgill TC. Demonstration of large peak-to-valley current ratios in InAs/AlGaSb/InAs single-barrier heterostructures. Appl Phys Lett 1989;55(13):1348–50.

[82] Soderstrom JR, Yao JY, Andersson TG. Observation of resonant tunneling in InSb/AlInSb double-barrier structures. Appl Phys Lett 1991;58(7):708–10.

[83] Beresford R, Luo LF, Wang WI. Narrow-Gap InAs for hetero-structure tunneling. Semicond Sci Technol 1990;5:S195–9.

[84] Collins DA, Yu ET, Rajakarunanayake Y, Soderstrom JR, Ting DZY, Chow DH, et al. Experimental-observation of negative differential resistance from an inas/gasb interface. Appl Phys Lett 1990;57(7):683–5.

[85] Luo LF, Beresford R, Longenbach KF, Wang WI. Resonant interband coupling in single-barrier heterostructures of InAs/GaSb/InAs and GaSb/InAs/GaSb. J Appl Phys 1990;68(6):2854–7.

[86] Yang L, Chen JF, Cho AY. A new GaSb/AlSb/GaSb/AlSb/InAs double-barrier interband tunneling diode and its tunneling mechanism. J Appl Phys 1990;68(6):2997–3000.

[87] Ting DZY, Collins DA, Yu ET, Chow DH, Mcgill TC. Large peak current densities in novel resonant interband tunneling heterostructures. Appl Phys Lett 1990;57(12):1257–9.

[88] Longenbach KF, Luo LF, Wang WI. Resonant interband tunneling in InAs/GaSb/AlSb/InAs and GaSb/InAs/AlSb/GaSb heterostructures. Appl Phys Lett 1990;57(15):1554–6.

[89] Houng MP, Wang YH, Shen CL, Chen JF, Cho AY. Improvement of peak-to-valley ratio by the incorporation of the InAs layer into the GaSb/AlSb/GaSb/AlSb/InAs double barrier resonant interband tunneling structure. Appl Phys Lett 1992;60(6):713–5.

[90] Chen JF, Cho AY. The effects of GaSb/InAs broken gap on interband tunneling current of a GaSb/AlSb/GaSb/AlSb/InAs tunneling structure. J Appl Phys 1992;71(9):4432–5.

[91] Chen JF, Cho AY. Interband tunneling between valence-band and conduction-band quantum-wells in a GaSb/AlSb/InAs/AlSb/GaSb/AlSb/InAs triple-barrier structure. J Appl Phys 1992;72(3):960–3.

[92] Brown ER, Parker CD. Resonant tunnel diodes as submillimetre-wave sources. Philos Trans Roy Soc A 1996;354(1717):2365–81.

[93] Diamond SK, Ozbay E, Rodwell MJW, Bloom DM, Pao YC, Harris JS. Resonant tunneling diodes for switching applications. Appl Phys Lett 1989;54(2):153–5.

[94] Goldman VJ, Tsui DC, Cunningham JE. Evidence for LO-phonon-emission-assisted tunneling in double-barrier heterostructures. Phys Rev B 1987;36(14):7635–7.

[95] Li J, Mirabedini A, Mawst LJ, Savage DE, Matyi RJ, Kuech TF. Effect of interface roughness on performance of AlGaAs/InGaAs/GaAs resonant tunneling diodes. J Cryst Growth 1998;195(1–4):617–23.

[96] Dellow MW, Beton PH, Langerak CJGM, Foster TJ, Main PC, Eaves L, et al. Resonant tunneling through the bound-states of a single donor atom in a quantum-well. Phys Rev Lett 1992;68(11):1754–7.

[97] Kitabayashi H, Waho T, Yamamoto M. Resonant interband tunneling current in InAs/AlSb/GaSb/AlSb/InAs double barrier diodes. J Appl Phys 1998;84(3):1460–6.

[98] Shen J. Mechanisms of valley currents in InAs/AlSb/GaSb resonant interband tunneling diodes. J Appl Phys 1995;78(10):6220–3.

[99] Xu YY, Fay P, Chow DH, Schulman JN. Experimental investigation of the temperature dependence of InAs–AlSb–GaSb resonant interband tunnel diodes. IEEE Trans Electron Dev 2004;51(7):1060–4.

[100] Tehrani S, SHen J, Goronkin H, Kramer G, Hoogstra M, Zhu TX. AlAs hole barriers in InAs/GaSb/AlSb interband tunnel diodes. In: Intl symp GaAs and related compounds. Inst Phys Conf Ser, vol. 136, 1993. p. 209–14.

[101] Shiralagi K, Shen J, Tsui R. Effects of layer design on the performance of InAs/AlSb/GaSb resonant interband tunneling diodes on GaAs substrates. J Electron Mater 1997;26(12):1417–21.

[102] Magno R, Bracker AS, Bennett BR, Twigg ME, Weaver BD. The effect of defects on InAs/AlSb/GaSb resonant tunneling diodes. In: Proc InP and related mater conf, 2000. p. 122–5.

[103] Magno R, Weaver BD, Bracker AS, Bennett BR. Proton irradiation of InAs/AlSb/GaSb resonant tunneling diodes. Appl Phys Lett 2001;78(17):2581–3.

[104] Schulman JN, Chow DH, Hasenberg TC. InAs/antimonide-based resonant-tunneling structures with ternary alloy layers. Solid-State Electron 1994;37(4–6):981–5.

[105] Magno R, Bracker AS, Bennett BR. Resonant interband tunnel diodes with AlGaSb barriers. J Appl Phys 2001;89(10):5791–3.

[106] Ozbay E, Bloom DM, Chow DH, Schulman JN. 1.7-Ps, Microwave, integrated-circuit-compatible InAs/AlSb resonant-tunneling diodes. IEEE Electron Dev Lett 1993;14(8):400–2.

[107] Soderstrom JR, Brown ER, Parker CD, Mahoney LJ, Yao JY, Andersson TG, et al. Growth and characterization of high-current density, high-speed InAs/AlSb resonant tunneling diodes. Appl Phys Lett 1991;58(3):275–7.

[108] Soderstrom JR, Chow DH, Mcgill TC. InAs/A1Sb double-barrier structure with large peak-to-valley current ratio—a candidate for high-frequency microwave devices. IEEE Electron Dev Lett 1990;11(1):27–9.

[109] Smet JH, Broekaert TPE, Fonstad CG. Peak-to-valley current ratios as high as 50-1 at room-temperature in pseudomorphic InGaAs/AlAs/InAs resonant tunneling diodes. J Appl Phys 1992;71(5):2475–7.

[110] Su YK, Chang JR, Lu YT, Lin CL, Wu KM, Wu ZX. Novel AlInAsSb/InGaAs double-barrier resonant tunneling diode with high peak-to-valley current ratio at room temperature. IEEE Electron Dev Lett 2000;21(4):146–8.

[111] McMorrow D, Magno R, Bracker AS, Bennett BR, Buchner S, Melinger JS. Charge-collection dynamics of AlSb–InAs–GaSb resonant interband tunneling diodes (RITDs). IEEE Trans Nucl Sci 2001;48(6):1973–9.

[112] Chow DH, Dunlap HL, Williamson W, Enquist S, Gilbert BK, Subramaniam S, et al. InAs/AlSb/GaSb resonant interband tunneling diodes and Au-on-InAs/AlSb-superlattice Schottky diodes for logic circuits. IEEE Electron Dev Lett 1996;17(2):69–71.

[113] Soderstrom JR, Chow DH, Mcgill TC. Observation of large peak-to-valley current ratios and large peak current densities in AlSb/InAs/AlSb double-barrier tunnel structures. J Appl Phys 1989;66(10):5106–8.

[114] Chow DH, Schulman JN. Intrinsic current bistability in InAs/AlGaSb resonant-tunneling devices. Appl Phys Lett 1994;64(1):76–8.

[115] Jimenez JL, Mendez EE, Li X, Wang WI. Resonant tunneling and intrinsic bistability in GaSb-based double barrier heterostructures. Solid-State Electron 1996;40(1–8):583–4.

[116] Brown ER, Eglash SJ, Turner GW, Parker CD, Pantano JV, Calawa DR. Effect of lattice-mismatched growth on InAs/AlSb resonant-tunneling diodes. IEEE Trans Electron Dev 1994;41(6):879–82.

[117] Nosho BZ, Weinberg WH, Barvosa-Carter W, Bennett BR, Shanabrook BV, Whitman LJ. Effects of surface reconstruction on III–V semiconductor interface formation: the role of III/V composition. Appl Phys Lett 1999;74(12):1704–46.

[118] Lin Y, Gonzalez EM, Mendez EE, Magno R, Bennett BR, Bracker AS. Magnetotunneling between two-dimensional electron gases in InAs–AlSb–GaSb heterostructures. Phys Rev B 2003;68(3):035311.

[119] Nomoto K, Taira K, Suzuki T, Hase I. Experimental evidence of surface conduction in AlSb-InAs tunneling diodes. J Appl Phys 1999;85(2):953–8.

[120] Nomoto K, Taira K, Suzuki T, Hase I, Hiroshima H, Komuro M. Diameter dependence of current–voltage characteristics of ultrasmall area AlSb-InAs resonant tunneling diodes with diameters down to 20 nm. Appl Phys Lett 1997;70(15):2025–7.

[121] Reed MA, Randall JN, Aggarwal RJ, Matyi RJ, Moore TM, Wetsel AE. Observation of discrete electronic states in a zero-dimensional semiconductor nanostructure. Phys Rev Lett 1988;60(6):535–7.

[122] Shiralagi K, Tsui R, Goronkin H, Pendharkar S, Tresek J, Allen S. Sidewall spacer defined resonant interband tunneling diodes. J Electron Mater 1998;27(1):L1–4.

[123] Williamson W, Enquist SB, Chow DH, Dunlap HL, Subramaniam S, Lei PM, et al. 12 GHz clocked operation of ultralow power interband resonant tunneling diode pipelined logic gates. IEEE J Solid-State Circ 1997;32(2):222–31.

[124] Shen J, Kramer G, Tehrani S, Goronkin H, Tsui R. Static random-access memories based on resonant interband tunneling diodes in the InAs/GaSb/AlSb material system. IEEE Electron Dev Lett 1995;16(5):178–80.

[125] Shen J, Tehrani S, Goronkin H, Kramer G, Tsui R. An exclusive-nor based on resonant interband tunneling FET's. IEEE Electron Dev Lett 1996;17(3):94–6.

[126] Fay P, Lu J, Xu Y, Bernstein GH, Gonzalez A, Mazumder P, et al. Digital integrated circuit using integrated InAlAs/InGaAs/InP HEMTs and InAs/AlSb/GaSb RITDs. Electron Lett 2001;37(12): 758–9.

[127] Bennett BR, Bracker AS, Magno R, Boos JB, Bass R, Park D. Monolithic integration of resonant interband tunneling diodes and high electron mobility transistors in the InAs/GaSb/AlSb material system. J Vac Sci Technol B 2000;18(3):1650–2.

[128] Ancona MG, Boos JB, Justh EW. Modeling of ultra-low-power AlSb/InAs HEMT-RITD circuits. In: Proc InP and related mater conf, 2000. p. 130–3.

[129] Hanbicki AT, Magno R, Cheng SF, Park YD, Bracker AS, Jonker BT. Nonvolatile reprogrammable logic elements using hybrid resonant tunneling diode-giant magnetoresistance circuits. Appl Phys Lett 2001;79(8):1190–2.

[130] Brown ER, Soderstrom JR, Parker CD, Mahoney LJ, Molvar KM, Mcgill TC. Oscillations up to 712 Ghz in InAs/AlSb resonant-tunneling diodes. Appl Phys Lett 1991;58(20):2291–3.

[131] Luo LF, Beresford R, Wang WI. Interband tunneling in poly-type GaSb/AlSb/InAs heterostructures. Appl Phys Lett 1989;55(19): 2023–5.

[132] Chen JF, Yang L, Wu MC, Chu SNG, Cho AY. On the effect of the barrier widths in the InAs/AlSb/GaSb single-barrier interband tunneling structures. J Appl Phys 1990;68(7):3451–5.

[133] Schulman JN, Chow DH. Sb-heterostructure interband backward diodes. IEEE Electron Dev Lett 2000;21(7):353–5.

[134] Fay P, Schulman JN, Thomas S, Chow DH, Boegeman YK, Holabird KS. High-performance antimonide-based heterostructure backward diodes for millimeter-wave detection. IEEE Electron Dev Lett 2002;23(10):585–7.

[135] Meyers RG, Fay P, Schulman JN, Thomas S, Chow DH, Zinck J, et al. Bias and temperature dependence of Sb-based heterostructure millimeter-wave detectors with improved sensitivity. IEEE Electron Dev Lett 2004;25(1):4–6.

[136] Vengurlekar AS, Capasso F, Chiu TH. Impact ionization in the base of a hot-electron AlSb/InAs bipolar-transistor. Appl Phys Lett 1990; 57(17):1772–4.

[137] Pekarik JJ, Kroemer H, English JH. An AlSb–InAs–AlSb double-heterojunction P-N-P bipolar-transistor. J Vac Sci Technol B 1992; 10(2):1032–4.

[138] Dodd PE, Lovejoy ML, Lundstrom MS, Melloch MR, Woodall JM, Pettit D. Demonstration of npn InAs bipolar transistors with inverted base doping. IEEE Electron Dev Lett 1996;17(4):166–8.

[139] Moran PD, Chow D, Hunter A, Kuech TF. Fabrication of InAs/ AlSb/GaSb heterojunction bipolar transistors on Al₂O₃ substrates by wafer bonding. Appl Phys Lett 2001;78(15):2232–4.

[140] Averett KL, Maimon S, Wu X, Koch MW, Wicks GW. InAs-based bipolar transistors grown by molecular beam epitaxy. J Vac Sci Technol B 2002;20(3):1213–6.

[141] Averett KL, Wu X, Koch MW, Wicks GW. Low-voltage InAsP/ InAs HBT and metamorphic InAs BJT devices grown by molecular beam epitaxy. J Cryst Growth 2003;251(1–4):852–7.

[142] Maimon S, Averett KL, Wu X, Koch MW, Wicks GW. InAs-based heterojunction bipolar transistors. Electron Lett 2002;38(7):344–6.

[143] Thomas SI, Elliott K, Chow DH, Shi B, Deelman P, Brewer P, et al. Fabrication and performance of InAs-based heterojunction bipolar transistors. In: Proc InP and related mater conf, 2003. p. 26–31.

[144] Rieh JS, Jagannathan B, Greenberg DR, Meghelli M, Rylyakov A, Guarin F, et al. SiGe heterojunction bipolar transistors and circuits toward terahertz communication applications. IEEE Trans Microw Theory 2004;52(10):2390–408.

[145] Kotani K, Yamabi R, Kawasaki T, Yanagisawa M, Yaegassi S, Yano H. High-speed and uniform self-aligned InGaAs/InP HBTs for 40 Gb/s fiber optic communications applications. Jpn J Appl Phys 1 2003;42(4B):2352–8.

[146] Monier C, Sawdai D, Cavus A, Sandhu R, Lange M, Wang J, et al. High indium content metamorphic (In,Al)As/(In,Ga)As heterojunc-

tion bipolar transistors. In: Proc InP and related mater conf, 2003. p. 32–5.

[147] Noori AM, Sandhu RS, Hayashi SL, Meserole ED, Hardev V, Cavus A, et al. Strain relaxation and surface roughness of InAlAs graded buffer layers grown on InP for 6.05 angstrom applications. J Vac Sci Technol B 2004;22(5):2303–8.

[148] Monier C, Cavus A, Sandhu RS, Lange MD, Cheng P, Chan B, et al. narrow-band-gap HBT technology for low-power, high-speed applications. In: GaAs mantech conf, 2004. p. 13.2.

[149] Magno R, Bennett BR, Ikossi K, Ancona MG, Glaser ER, Papanicolaou N, et al. Antimony-based quaternary alloys for high-speed low-power electronic devices. Eastman conf, 2002. p. 288–96.

[150] Wang SH, Mohney SE, Hull BA, Bennett BR. Design of a shallow thermally stable ohmic contact to p-type InGaSb. J Vac Sci Technol B 2003;21(2):633–40.

[151] Wang SH, Mohney SE, Robinson JA, Bennett BR. Sulfur passivation for shallow Pd/W/Au ohmic contacts to p-InGaSb. Appl Phys Lett 2004;85(16):3471–3.

[152] Wang SH, Robinson JA, Mohney SE, Bennett BR. Shallow and thermally stable Pt/W/Au Ohmic contacts to p-type InGaSb. J Vac Sci Technol A 2005;23(2):293–7.

[153] Magno R, Boos JB, Campbell PM, Bennett BR, Glaser ER, Tinkham BP, et al. InAlAsSb/InGaSb double heterojunction bipolar transistor. Electron Lett 2005;41(6):370–1.

[154] Brar B, Bergman J, Pierson R, Rowell P, Nagy G, Sullivan G. Low-voltage AlGaSb/InAs/AlGaSb pnp HBTs. In: Dev res conf, 2003. p. 91–2.

[155] Bolognesi CR, Matine N, Dvorak MW, Yeo P, Xu XG, Watkins SP. InP/GaAsSb/InP double HBTs: a new alternative for InP-based DHB. IEEE Trans Electron Dev 2001;48(11):2631–9.

[156] Dvorak MW, Bolognesi CR, Pitts OJ, Watkins SP. 300 GHz InP/ GaAsSb/InP double HBTs with high current capability and $BV_{CEO} > = 6$ V. IEEE Electron Dev Lett 2001;22(8):361–3.

[157] Rajavel RD, Hussain T, Montes MC, Sawins MW, Thomas S, Chow DH. Molecular beam epitaxial growth and characterization of InP/GaAsSb/InP double heterojunction bipolar transistors. J Cryst Growth 2003;251(1–4):848–51.

[158] Chau R, Datta S, Doczy M, Doyle B, Jin J, Kavalieros J, et al. Benchmarking nanotechnology for high-performance and low-power logic transistor applications. IEEE Trans Nanotechnol 2005;4(2):153–8.

[159] Vurgaftman I, Meyer JR. Ferromagnetic resonant interband tunneling diode. Appl Phys Lett 2003;82(14):2296–8.

[160] Moon JS, Chow DH, Schulman JN, Deelman P, Zinck JJ, Ting DZY. Experimental demonstration of split side-gated resonant interband tunneling devices. Appl Phys Lett 2004;85(4):678–80.

[161] Yamada S, Kikutani T, Gozu S, Sato Y, Kita T. Spontaneous spin-splitting observed in resonant tunneling diode with narrow band-gap asymmetric quantum well. Physica E 2002;13(2–4):815–8.

[162] Koga T, Nitta J, Takayanagi H. Spin-filter device based on the Rashba effect using a nonmagnetic resonant tunneling diode. Phys Rev Lett 2002;88(12):126601.

[163] Petukhov AG, Demchenko DO, Chantis AN. Electron spin polarization in resonant interband tunneling devices. Phys Rev B 2003; 68(12):125332.

[164] Woolard D, Zhang WD, Gelmont B. A novel interband-resonant tunneling diode (I-RTD) based high-frequency oscillator. Solid-State Electron 2005;49(2):257–66.

[165] Yang CH, Yang MJ, Cheng KA, Culbertson JC. A novel InAs quantum wire system. Physica E 2003;17(1–4):161–3.

[166] Fuchs F, Weimer U, Pletschen W, Schmitz J, Ahlswede E, Walther M, et al. High performance InAs/GaInSb superlattice infrared photodiodes. Appl Phys Lett 1997;71(22):3251–3.

[167] Meyer JR, Hoffman CA, Bartoli FJ, Rammohan LR. Type-II quantum-well lasers for the midwavelength infrared. Appl Phys Lett 1995;67(6):757–9.